

# Computable Stability for Persistence Rank Function Machine Learning

Qiquan Wang<sup>1</sup>, Inés García-Redondo<sup>1,2‡</sup>, Pierre Faugère<sup>3</sup>,  
Anthea Monod<sup>1,†</sup>, and Gregory Henselman-Petrusek<sup>4</sup>

Corresponding e-mails: <sup>†</sup>a.monod@imperial.ac.uk, <sup>‡</sup>i.garcia-redondo22@imperial.ac.uk

## Abstract

Persistent homology barcodes and diagrams are a cornerstone of topological data analysis. Widely used in many real data settings, they relate variation in topological information (as measured by cellular homology) with variation in data, however, they are challenging to use in statistical settings due to their complex geometric structure. In this paper, we revisit the persistent homology rank function—an invariant measure of “shape” that was introduced before barcodes and persistence diagrams and captures the same information in a form that is more amenable to data and computation. In particular, since they are functions, techniques from functional data analysis—a domain of statistics adapted for functions—apply directly to persistent homology when represented by rank functions. Rank functions, however, have been less popular than barcodes because they face the challenge that stability—a property that is crucial to validate their use in data analysis—is difficult to guarantee, mainly due to metric concerns on rank function space. However, rank functions extend more naturally to the increasingly popular and important case of multiparameter persistent homology. In this paper, we study the performance of rank functions in functional inferential statistics and machine learning on both simulated and real data, and in both single and multiparameter persistent homology. We find that the use of persistent homology captured by rank functions offers a clear improvement over existing approaches. We then provide theoretical justification for our numerical experiments and applications to data by deriving several stability results for single- and multiparameter persistence rank functions under various metrics with the underlying aim of computational feasibility and interpretability.

## 1 Introduction

Topological data analysis (TDA) is a field within data science that leverages theory from algebraic topology to computational and data analytic settings and which has enjoyed great success in many other sciences, including biology, physics, economics, social sciences, materials science, to name a few. A cornerstone methodology of TDA is *persistent homology*, which is computed from input data and produces a summary statistic of such data. Key properties of persistent homology that make it so widely usable are its flexibility to adapt to a wide range of complex data structures (including those that do not exhibit a metric space structure, such as networks); its interpretability within the scientific domains where data arise; and its stability, which is the focus of this work. Stability is an important property that is required to guarantee the validity of conclusions drawn from data analysis using persistent homology; it provides a notion of faithfulness of the topological representation of the input data. Specifically, it guarantees that a bounded perturbation of the input data results in a bounded perturbation of their summary statistics captured by persistent homology.

---

<sup>1</sup>Department of Mathematics, Imperial College London, UK

<sup>2</sup>London School of Geometry and Number Theory, University College London, UK

<sup>3</sup>Department of Mathematics, ENS Lyon, France

<sup>4</sup>Pacific Northwest National Laboratory, Richland, Washington, USA

Persistent homology has its roots in various constructions and thus has various representations; the most well-known is the *persistence diagram* or equivalently, the *barcode*. A less-used representation is the *rank function*, initially proposed in the early 1990s by Frosini (1992) as the *size function*. Although rank functions (as size functions) were proposed before persistence diagrams and barcodes, and they are in fact equivalent to persistence diagrams and barcodes, their use has been comparatively restricted due to the difficulty in establishing stability results. This difficulty arises from the challenge of selecting an appropriate metric to measure distances between rank functions. With the generalization of persistent homology to *multiparameter persistent homology*, rank functions are becoming increasingly relevant and important as they extend naturally to the multiparameter setting where persistence diagrams and barcodes do not. Additionally, rank functions are naturally amenable to *functional data analysis* (FDA)—a well-established and well-developed field within statistics—which persistence diagrams and barcodes are not. Rank functions, as opposed to persistence diagrams and barcodes, are functions and FDA is a toolbox of methods for data that take the form of functions. Thus, rank functions are important for both their natural extension to multiparameter persistence as well as for the potential that they open for the application of a vast and powerful set of FDA tools. In this paper, we return to rank functions and study their performance as representations for persistent homology in statistics and machine learning tasks using FDA. Specifically, we study both single and multiparameter persistent homology in inferential machine learning, on both simulated and real data, and find a clear improvement in performance using rank functions compared to existing methods. We then validate these results by deriving several stability results for both single and multiparameter persistence; we also introduce a new pseudometric with which we establish stability for rank functions in the multiparameter setting.

The remainder of this paper is organized as follows. We close this introductory section with an overview of existing literature associated to our work. In Section 2, we introduce rank functions and discuss their relation to barcodes and persistence diagrams, as well as various metrics associated to these representations of persistent homology and their implications in stability. In Section 3, we present several implementations of rank functions in inferential tasks using FDA in statistics and machine learning methods, on both real and simulated data. We then justify our findings in Section 4, where we present various stability results in both the single and multiparameter settings. Our focus is on *computable* stability, since our interest is to validate our conclusions from our previous data analyses; the emphasis is therefore on establishing stability with respect to computable metrics. We close with a discussion in Section 5 on our findings and propose directions for future research.

**Related Work.** From the perspective of applications and data analysis, FDA methods have been previously used in TDA by Crawford et al. (2020), who perform Gaussian process regression using a dynamic version of the Euler characteristic—a topological invariant that shares the same nature of persistent homology. Robins and Turner (2016) propose principal component analysis (PCA) for rank functions specifically. PCA is an important dimension reduction technique in descriptive statistics, which is used an exploratory procedure to gain insights on an observed dataset. In our work, we aim to establish inferential (as opposed to descriptive) methods for rank functions to provide insight on the often unknown data generating process and the general, infinite population.

From the theoretical perspective, rank functions were introduced as size functions and used as a mathematical tool for shape and image analysis in computer vision and pattern recognition (Verri et al., 1993; Frosini and Landi, 1999; Landi and Frosini, 2002; Biasotti et al., 2008; Di Fabio et al., 2009). With the extension of size functions to algebraic topology (Frosini and Landi, 1999; Cagliari et al., 2001) came the development of *size theory* (see Biasotti et al. (2008) for a survey). In particular, the concepts of *size homotopy groups* and *size functors* were defined, which were then later re-termed to rank function theory. The algebraic topolog-

ical formulations of rank functions directly coincide with parallel concepts from persistent homology and, as will be discussed further on, rank function theory and persistent homology capture identical topological information and in this sense, are equivalent.

Stability for persistent homology has been firmly established with respect to various rigorous metrics for persistence diagrams and barcodes, which will be discussed in greater detail in Section 2.3. Measures of distance for rank or size functions are, in contrast, *pseudometrics*, where the condition of identity of indiscernibles is relaxed. Such pseudometrics were constructed using a correspondence between size functions and formal series (Frosini and Landi, 2001) to circumvent the absence of the a barcode decomposition, which lends interpretability to applications (Landi and Frosini, 1997). Such a correspondence is obtained by studying the domain of discontinuities of size functions to trace back to the points from the persistence diagram and their multiplicities as corner points (or vertical lines in the case of essential cycles).

Three extended pseudometrics on size functions (Landi and Frosini, 1997) are relevant to our work: the *deformation distance*, more widely known today under the name of 1-Wasserstein distance between the associated persistence diagrams; the *Hausdorff pseudo-distance*, which gave rise to the bottleneck distance between persistence diagrams; and the  $L^p$  *pseudo-distance*, which exhibits an unstable nature and did not appear to inspire any well-known distance. Notions of pseudo-stability have been established for size functions under these pseudometrics, whose ideas and techniques reappear later in the currently widely-known stability results for persistent homology. In particular, it is worth noting that d’Amico et al. (2003) and d’Amico et al. (2010) renamed the Hausdorff pseudo-distance to the *matching distance* to emphasize the fact that its computation amounts to finding an optimal matching between multisets, as the bottleneck distance does and which was used in establishing the first results of stability for persistence. They then proved that it is stable under noisy perturbations when restricted to *reduced* size functions.

More recently, Skraba and Turner (2021) studied the stability properties of *weighted*  $L^p$  metrics on rank functions. Considering weighted metrics, however, results in studying an entirely different problem, as will be discussed at the beginning of Section 4.

## 2 Persistent Homology and Rank Functions

In this section, we lay the foundations for our work by introducing the essential background to the theory of persistent homology and their metrics.

### 2.1 Persistence Modules and Rank Invariants

The algebraic object that is the central focus of persistent homology theory is the *persistence module*, which formally is a functor mapping from a poset category to the category of vector spaces,  $M : (\mathbb{P}, \leq) \rightarrow \mathbf{Vec}$ , also written as  $M \in \mathbf{Vec}^{(\mathbb{P}, \leq)}$  (Bubenik and Scott, 2014; Bubenik et al., 2015; Kim and Mémoli, 2021). Further, assuming that  $\mathbf{Vec}$  is the category of finite dimensional vector spaces, we obtain *pointwise finite dimensional* (p.f.d.) persistence modules, which will be studied in this work.

Arguably, the most relevant example is the module of persistent homology for a finite simplicial complex, first introduced by Edelsbrunner et al. (2002) and obtained as follows. Consider a *filtration*, i.e., a diagram  $F \in \mathbf{Simp}^{(\mathbb{R}, \leq)}$  such that  $F_x := F(x)$  is a finite simplicial complex for each  $x \in \mathbb{R}$ , and such that for any other  $y \in \mathbb{R}$  with  $x \leq y$ ,  $F(x \leq y)$  is an inclusion  $F_x \subset F_y$ . Given that we are considering finite simplicial complexes, there is a finite discrete set of values in which the filtration changes. For each  $k \geq 0$ , we obtain another diagram  $H_k(F) \in \mathbf{Vec}^{(\mathbb{R}, \leq)}$  by setting

$$H_k(F)(x) := H_k(F_x, \mathbb{F}),$$

where  $H_k : \text{Simp} \rightarrow \text{Vec}$  is the homology functor of order  $k \geq 0$  with coefficients over a field  $\mathbb{F}$ . We shall also refer to the diagram given by

$$H(F)(x) := H(F_x, \mathbb{F}) = \bigoplus_{k \geq 0} H_k(F_x, \mathbb{F})$$

using the notation  $H(F) \in \text{Vec}^{(\mathbb{R}, \leq)}$ .

The p.f.d. persistence module  $H(F) \in \text{Vec}^{(\mathbb{R}, \leq)}$  is called the *persistent homology* module of the filtration. Observe that we obtain a spectrum of linear maps connecting the vector spaces, and thus, a natural way to study its structure is to consider the *ranks* of these maps. Let  $\mathbb{R}^{2+} := \{(x, y) \in (\{-\infty\} \cup \mathbb{R}) \times (\mathbb{R} \cup \{\infty\}) : x \leq y\}$ .

**Definition 1** (Rank function). Given the p.f.d. persistence module  $H(F) \in \text{Vec}^{(\mathbb{R}, \leq)}$ , its *rank function* is defined as

$$\begin{aligned} \beta^{H(f)} : \mathbb{R}^{2+} &\rightarrow \mathbb{Z} \\ (x, y) &\mapsto \text{rank } H(F)(x \leq y) = \dim \text{Im} (H(F)(x \leq y)). \end{aligned}$$

The space of rank functions will be denoted by  $\mathcal{I}_1$ .

There is an important distinction between *single-parameter* persistence modules, i.e., diagrams such as those we have considered so far  $M \in \text{Vec}^{(\mathbb{R}, \leq)}$ , and *multiparameter* persistence modules (Carlsson and Zomorodian, 2009), i.e., diagrams which allow indexing over the poset  $(\mathbb{R}^n, \preceq)$ . Here,  $\preceq$  is the product order inherited from the partial order in the reals, namely  $(x_1, \dots, x_n) \preceq (y_1, \dots, y_n)$  if  $x_i \leq y_i$  for all  $i = 1, \dots, n$ . The construction discussed above that gives rise to persistent homology can be replicated for these posets to obtain *multifiltrations* and thus, *multiparameter persistent homology*. Rank functions are also generalizable to multiparameter persistence in a natural way. Let  $\mathbb{R}^{2n+} := \{(x, y) \in (\{-\infty\} \cup \mathbb{R})^n \times (\mathbb{R} \cup \{\infty\})^n : x \preceq y\}$ .

**Definition 2** (Rank invariant). Given the p.f.d. multiparameter persistence module  $H(F) \in \text{Vec}^{(\mathbb{R}^n, \preceq)}$ , its *rank invariant* is defined as

$$\begin{aligned} \beta^{H(f)} : \mathbb{R}^{2n+} &\rightarrow \mathbb{Z} \\ (x, y) &\mapsto \text{rank } H(F)(x \preceq y) = \dim \text{Im} (H(F)(x \preceq y)). \end{aligned}$$

The space of rank invariants for  $n$ -dimensional persistence modules will be denoted by  $\mathcal{I}_n$ .

A *complete invariant* is a specific invariant assigned to a persistence module; it is the same invariant for all isomorphic persistence modules and different for non-isomorphic ones. One of the main differences between single-parameter and multiparameter persistence is the existence of complete invariants: rank functions are complete, discrete invariants for single-parameter persistence, and, as we will see next, they are equivalent to persistence diagrams and persistent homology barcodes in the single-parameter setting.

## 2.2 Persistence Diagrams and Barcodes

In single-parameter persistence, rank functions are equivalent to *persistence diagrams* and *barcodes*—two complete, discrete invariants obtained from the following distinct approaches.

**By Images: Persistence Diagrams.** Persistence diagrams can be traced back to the study of discontinuities of rank functions by Frosini and Landi (2001). Edelsbrunner et al. (2002) then reinterpreted these ideas to obtain diagrams that visually and interpretably capture the persistent homology of a filtered simplicial complex  $F \in \text{Simp}^{(\mathbb{R}, \leq)}$ .

Let  $T = \{t_1, \dots, t_\ell\} \subset \mathbb{R}$  be the discrete set of values over which the filtration changes, and consider a sequence  $\{s_0, s_1, \dots, s_\ell\}$  of real numbers interleaved with the elements of  $T$ :  $s_{i-1} \leq t_i \leq s_i$ . Also, set  $s_{-1} = t_0 = -\infty$  and  $s_{\ell+1} = t_{\ell+1} = +\infty$  and call  $\overline{T} = T \cup \{-\infty, +\infty\}$ . Lastly, let

$$\mu_i^j := \beta(s_{i-1}, s_j) - \beta(s_i, s_j) + \beta(s_i, s_{j-1}) - \beta(s_{i-1}, s_{j-1}). \quad (1)$$

**Definition 3.** The *persistence diagram* of  $H(F)$  is the finite multiset of points given by

$$\text{Dgm}(F) := \{(t_i, t_j) \in \overline{T} \times \overline{T} : t_i < t_j\},$$

where each point  $(t_i, t_j)$  has multiplicity  $\mu_i^j$ , union all the points in the diagonal  $\partial = \{(x, y) \in \mathbb{R}^{2+} : x = y\}$  counted with infinite multiplicity. The space of persistence diagrams is denoted by  $\mathcal{D}$ .

**By Indecomposables: Barcodes.** The Structure Theorem due to Zomorodian and Carlsson (2005) (with the version in full generality due to Crawley-Boevey (2015) and Botnan and Crawley-Boevey (2020)) asserts that the module  $H(F)$  is isomorphic to a finite direct sum of indecomposable persistence modules

$$H(F) \simeq M_1(F) \oplus \cdots \oplus M_m(F)$$

and that any two ways of writing  $H(F)$  as a sum of indecomposables are the same, up to a reordering of the indecomposables. For single-parameter persistence, each  $M_j(F)$  is an *interval persistence module*, i.e., there is a pair of values  $b_j < d_j$ , where  $d_j$  may be infinite, such that  $M_j(F)(x)$  is a copy of the field for all values  $b_j \leq x < d_j$  and zero elsewhere. We denote these persistence modules by  $\mathbb{I}[b_j, d_j]$ . In this setting, Zomorodian and Carlsson (2005) and Carlsson and de Silva (2010) define the barcode as follows.

**Definition 4.** The *barcode* of  $H(F)$  is the list of indecomposables given by the Structure Theorem, or equivalently, the collection of intervals that define these indecomposables

$$\text{Bar}(F) := \{[b_j, d_j) : M_j(F)(x) \text{ is nontrivial for } b_j \leq x < d_j\}.$$

**Equivalence between Persistence Diagrams, Barcodes, and Rank Functions.** A barcode translates to a persistence diagram by plotting the left endpoint versus the right endpoint of each interval persistence module. A persistence diagram translates to a barcode by turning each point  $(x, y)$  with  $x < y$  in the persistence diagram into an interval persistence module starting at  $x$  and ending at  $y$ . In this way, the persistence diagram is equivalent to a barcode, although the two definitions arise from two very different approaches.

Rank functions are also in bijection with persistence diagrams and barcodes. As seen above, rank functions are essential for the definition of the persistence diagram as they give one of the directions of the bijection. Moreover, they can be seen as cumulative functions on the persistence diagrams: the value of the rank function  $\beta^{H(F)}(x, y)$  corresponds to the number of points (counted with multiplicities) in the region  $(-\infty, x] \times [y, \infty)$  of the persistence diagram, providing the converse direction of the bijection.

An alternative approach to this equivalence can be seen through (1), recognizing it as a special case of a *Möbius inversion* (Patel, 2018), which also gives rise to a bijection between the space of barcodes and the space of rank functions. To see this, first recall that every partial order admits a linear extension (Szpilrajn, 1930) in the sense that for every partial order, there exists a compatible linear order.

A finite poset  $(P, \leq)$  with elements in  $P$  labeled as  $\{1, \dots, N\}$  can then be expressed by an upper triangular matrix  $\nu(P)$  with entries given by

$$(\nu(P))_{ij} := \begin{cases} 1 & \text{if } i \leq j, \\ 0 & \text{otherwise.} \end{cases}$$

By reflexivity of the partial order, the elements in the diagonal of the matrix are 1, so the matrix  $\nu(P)$  is always invertible. The *Möbius transform* over the poset is then defined as

$$\mu(P) := \nu(P)^{-1}.$$

*Example 5.* Consider the poset with a partial order and its corresponding linearization in Figure 1. For this poset, we have

$$\nu(\mathbf{P}) = \begin{pmatrix} 1 & 1 & 1 & 1 & 1 \\ & 1 & 1 & 1 & 1 \\ & & 1 & 0 & 0 \\ & & & 1 & 0 \\ & & & & 1 \end{pmatrix}$$

and thus the Möbius transform for this poset is

$$\mu(\mathbf{P}) = \begin{pmatrix} 1 & -1 & 0 & 0 & 0 \\ & 1 & -1 & -1 & -1 \\ & & 1 & 0 & 0 \\ & & & 1 & 0 \\ & & & & 1 \end{pmatrix}.$$

Returning to barcodes and rank functions, we consider the partially ordered set of intervals  $\mathbf{P} = \{(a, b) \subset \mathbb{R} \times (\mathbb{R} \cup \{\infty\})\}$  with order induced by the inclusion  $\supseteq$ . The barcode of a persistence module can be seen as a function  $\mathbf{B} : \mathbf{P} \rightarrow \mathbb{Z}$  which, for each interval  $(a, b)$ , outputs the number of times such interval appears in the barcode. In the same way, the rank function of the persistence module can be considered as a function  $\beta : \mathbf{P} \rightarrow \mathbb{Z}$  which, for each interval  $(a, b)$ , outputs the *rank* of the map corresponding to  $a \leq b$  in the persistence module. Patel (2018) proves that the rank function satisfies the following Möbius inversion formula

$$\beta = \nu(\mathbf{P}) \cdot \mathbf{B},$$

which for a given interval  $(a, b)$ , amounts to

$$\beta(a, b) = \sum_{[c, d] \in \mathbf{P}: [c, d] \supseteq [a, b]} \mathbf{B}([c, d]).$$

Möbius formulas are invertible, giving the converse direction of the equivalence between barcodes and rank functions,

$$\mathbf{B} = \mu(\mathbf{P}) \cdot \beta. \tag{2}$$

**Generalizing Persistence Diagrams and Barcodes to Multiparameter Persistence.** The Structure Theorem can be extended to general p.f.d. persistence modules indexed over a small category (Botnan and Crawley-Boevey, 2020), which includes the case of multiparameter persistence. As seen above, for single-parameter persistence, it turns out that the only possible indecomposables are interval modules, i.e., modules  $\mathbb{I}[b, d]$  defined over intervals with  $b \leq d \in \mathbb{R}$ , as introduced before. For a general poset, we have the following definition.

**Definition 6.** An *interval of a poset*  $\mathbf{P}$  is a nonempty subset  $I \subset \mathbf{P}$  such that:

1. for any  $x, y \in I$  and  $x \leq z \leq y$ ,  $z \in I$ ;
2. and for any  $x, y \in I$ , there is a sequence  $x = z_0, \dots, z_m = y \in I$  such that  $z_i$  and  $z_{i+1}$  are comparable for all  $0 \leq i \leq m - 1$ .

The characterization of the indecomposables in single-parameter persistence as interval modules allows for the interpretability of births and deaths of topological features within barcodes and persistence diagrams. For multiparameter persistence, however, there is a wider and much more complicated selection of possible indecomposables for which there is no natural, parallel definition of barcode (Carlsson and Zomorodian, 2007).

A focal interest of the literature on multiparameter persistence is the development of interpretable and computable invariants for multiparameter persistence modules. An approach often followed capitalizes the *multigraded* structure of the persistence modules, which is based on the observation that  $n$ -dimensional persistence modules can be seen as  $n$ -graded modules over a ring of polynomials (Carlsson and Zomorodian, 2007), for which variants already exist. In this context, the main issue is to understand how interpretable and computationally feasible these existing invariants are in the persistence setting. In that vein, Lesnick and Wright (2015, 2022) propose an efficient algorithm to compute minimal presentations of biparameter ( $n = 2$ ) persistence modules, from which multigraded Betti numbers and Hilbert functions are readily obtained, while Harrington et al. (2019) suggest multigraded Hilbert series, multigraded associated primes, and local cohomology as invariants for studying multiparameter persistence.

There have also been efforts to redefine the notion of a barcode in multiparameter persistence without using the Structure Theorem: Miller (2020) developed a theory of modules over posets, giving rise to “QR codes” (as an extension of barcodes) in multiparameter persistence, and very recently, *signed* barcodes (Botnan et al., 2022) have been introduced as multiparameter persistence invariants. Signed barcodes are closely related to the rank invariant; they are encoded as a  $\mathbb{Z}$ -linear combination of rank invariants of indicator modules on segments in the underlying poset.

To the best of our knowledge and at the time of research, only the approach by Lesnick and Wright (2015, 2022) is implemented in the publicly available RIVET software (The RIVET Developers, 2020). The algorithm proposed in RIVET was later optimized by Kerber and Rolle (2021), which is also publicly available.

In this work, we focus on rank invariants as a natural and easily generalizable invariant for the study of higher dimensional modules, which also turns out to be the invariant originally proposed by Carlsson and Zomorodian (2007) for higher dimensional studies. The property of rank invariants that is the most fundamental for our goals in this paper is that they can be easily computed using RIVET. Moreover, the reinterpretation of (1) as a Möbius inversion showcases the intrinsic connection between rank functions and persistence diagrams. Consequently, one strategy to generalize persistence diagrams, bypassing decomposition theorems, is to generalize rank functions and then define the diagrams as their Möbius inversion. This is the approach taken by Patel (2018) and Kim and Mémoli (2021). More precisely, Kim and Mémoli (2021) introduced *generalized rank invariants* for persistence modules  $F : \mathbb{P} \rightarrow \mathbb{C}$  where  $\mathbb{P}$  is essentially a finite poset and  $\mathbb{C}$  is essentially a small, symmetric, monoidal, bicomplete category with images. In particular, the implication is that for interval decomposable modules, the generalized rank invariant is a complete invariant (Kim and Mémoli, 2021).

*Remark 7.* When  $\text{Vec}$  is equipped with the usual direct sum operation (the one used for the decomposition theorems of persistence modules), it satisfies all the properties of the target category of the generalized persistence diagrams. Moreover,  $(\mathbb{Z}, \leq)$  is essentially finite and any finite poset is also essentially finite. However  $(\mathbb{R}, \leq)$  or even  $(\mathbb{Z}_{\geq 0}^n, \leq)$  for  $n > 1$  are not necessarily finite, so the setting of Kim and Mémoli (2021) does not apply to multiparameter persistence in full generality.

## 2.3 Metrics and Stability in Persistence

Stability results give bounds for metrics defined on invariants of persistence modules, showing that such invariants are robust to noise. It is a fundamental property that is crucial to the use of persistent homology in data analysis; a more detailed review of the existing stability results can be found in (Cao and Monod, 2022a, Section 2.3). Defining the appropriate metrics and understanding their properties are central questions when faced with asserting stability.

**Metrics on Barcodes and Persistence Diagrams.** We recall the most widely used metrics to compare persistence diagrams and their stability properties in single-parameter persistence. These metrics in particular are computable and most relevant in real data applications.

**Definition 8.** The *bottleneck distance* between the persistence diagrams  $D_1$  and  $D_2$  is defined as

$$d_B(D_1, D_2) := \inf_{\phi: D_1 \rightarrow D_2} \sup_{x \in D_1} \|x - \phi(x)\|_\infty,$$

where  $\|\cdot\|_\infty$  is the infinity norm  $\ell^\infty$  on  $\mathbb{R}^2$  and  $\phi$  ranges over all bijections between  $D_1$  and  $D_2$ .

The most prominent stability result concerns the bottleneck distance and is due to Cohen-Steiner et al. (2007), who proved that the map sending a tame function  $f : X \rightarrow \mathbb{R}$  defining a filtration  $F(x) := f^{-1}(-\infty, x]$  to its persistence diagram  $\text{Dgm}(F)$  (also denoted  $\text{Dgm}(f)$ ) is 1-Lipschitz with respect to the bottleneck distance for diagrams and the  $L^\infty$  distance for functions. This result was the first Stability Theorem for persistent homology and justified much of the interest in using this metric in real data applications.

The bottleneck distance can be extended by replacing  $\ell^\infty$  with  $\ell^p$  norms, which give a stronger sense of proximity.

**Definition 9.** For  $1 \leq p < \infty$  and  $1 \leq q \leq \infty$  we define the  *$p, q$ -Wasserstein distance* between two persistence diagrams  $D_1$  and  $D_2$  as

$$W_{p,q}(D_1, D_2) := \inf_{\phi: D_1 \rightarrow D_2} \left[ \sum_{x \in D_1} \|x - \phi(x)\|_q^p \right]^{1/p}$$

where  $\|\cdot\|_q$  is the  $\ell^q$  norm on  $\mathbb{R}^2$  and  $\phi$  ranges over all bijections between  $D_1$  and  $D_2$ .

*Remark 10.* In this work we assume  $p = q$  and refer to this metric simply as the  $p$ -Wasserstein distance  $W_p$ .

Wasserstein metrics are widely used in applications, since they give a more accurate notion of proximity, especially  $p$ -Wasserstein distances with  $p = 1, 2$ , and have proven themselves to be more useful than the bottleneck distance in a number of instances. To name a few: Bramer and Wei (2020) show that  $p, \infty$ -Wasserstein metrics provide more accurate results when comparing two conjugate point clouds obtained using atom-specific persistent homology (Cang and Wei, 2017; Cang et al., 2018) in protein flexibility analysis. Gamble and Heo (2010) explore the power of the Wasserstein distance in the context of statistical analysis of landmark-shape data. Gidea (2017) shows that the  $W_{2,\infty}$  distance is able to detect premature evidence for critical transitions in financial data. Finally, Hamilton et al. (2022) study barcodes endowed with Wasserstein distances for protein folding data and compare them with the Gaussian integral tuned (Burley et al., 2021) vector representation.

Despite the desirable performance of Wasserstein distances in applications, their stability properties have not been as broadly studied until recently by Skraba and Turner (2021), who in particular establish the following cellular Wasserstein Stability Theorem for  $p$ -Wasserstein metrics, validating many of the existing results in applications and justifying their continued use.

**Theorem 11** (Cellular Wasserstein Stability Theorem, Skraba and Turner (2021)). *Let  $f, g : K \rightarrow \mathbb{R}$  be monotone functions on a finite CW-complex  $K$ . Then*

$$W_p(\text{Dgm}(f), \text{Dgm}(g)) \leq \|f - g\|_\infty.$$

The existence of this result also serves our study of the computational stability of rank functions using Wasserstein metrics.



In other words,  $d_B \leq d_I$ . In single-parameter persistence, the *Isometry Theorem* (Lesnick, 2015, Theorem 3.4) allows for the conclusion that in fact,  $d_B = d_I$ . Importantly for the extension to multiparameter persistence, Bauer and Lesnick (2015) provided a new proof of the Isometry Theorem using a reformulation of the bottleneck distance in terms of a matching induced by the interleaving distance, which also appears in Chazal et al. (2009).

**Metrics for Multiparameter Persistence.** As a metric defined directly on persistence modules, the interleaving distance can be naturally generalized to multiparameter persistence and it is, to date, the most prominent distance used in this setting. A desirable feature of the interleaving distance is that it satisfies a *universality* property, meaning it generalizes a stability property coming from the bottleneck distance in single-parameter persistence, and it bounds *any* other metric satisfying the same stability property from above (Lesnick, 2015, Corollary 5.6). Although this is a significant theoretical advantage, in computational terms, the interleaving distance is known to be NP-hard to compute except in the classic case of functors from  $\mathbb{Z}$  to  $\mathbf{Vec}$  (where it reduces to simply the bottleneck distance) (Bjerkevik et al., 2020), which restricts its applicability to real data applications. Note that checking for 0-interleaving (i.e., isomorphism) can be done in polynomial time for an arbitrary poset  $P$  (Bjerkevik et al., 2020).

In contrast to the interleaving distance, the combinatorial definitions of the bottleneck and Wasserstein metrics make them amenable to computation by nature. For an interval decomposable module (see Definition 6), partial matchings between the set of intervals appearing in the decomposition may be used to extend these distances to the multiparameter setting. This is the approach taken by Bjerkevik (2021) to generalize the definition of bottleneck distance in terms of induced partial matchings from Bauer and Lesnick (2015); Chazal et al. (2016).

**Definition 14.** Let  $M, N : \mathbb{R}^n \rightarrow \mathbf{Vec}$  be modules decomposing in the intervals  $\{J_j : j \in \mathcal{J}\}$ , and  $\{K_k : k \in \mathcal{K}\}$ . The *bottleneck distance* between  $M$  and  $N$  is defined as

$$d_B(M, N) = \inf_{\phi: \mathcal{I} \rightarrow \mathcal{K}} \max \left( \sup_{\phi(i)=k} d_I(\mathbb{I}^{J_i}, \mathbb{I}^{K_k}), \sup_{j \in \mathcal{J} \setminus \mathcal{I}} d_I(\mathbb{I}^{J_j}, 0), \sup_{k \in \mathcal{K} \setminus \phi(\mathcal{I})} d_I(0, \mathbb{I}^{K_k}) \right)$$

where  $\phi$  ranges over all injections of subsets  $\mathcal{I} \subset \mathcal{J}$  into  $\mathcal{K}$ .

Notice that for interval decomposable modules, we get  $d_I(M, N) \leq d_B(M, N)$  from the definition. Bjerkevik (2021) provided bounds for particular types of intervals which reversed the previous inequality. The following theorem is of particular interest in our work.

**Theorem 15.** (Bjerkevik, 2021, Theorem 4.3) For  $M, N \in \mathbf{Vec}^{(\mathbb{R}^n, \preceq)}$  rectangle decomposable modules, we have

$$d_B(M, N) \leq (2n - 1) \cdot d_I(M, N).$$

This bound is tight for  $n = 2$ , but improving it for  $n \geq 3$  remains open.

Concerning the extension of Wasserstein distances, one of the first approaches is due to Bubenik et al. (2023). Here, we follow their approach for interval decomposable multiparameter persistence modules equipped with the interleaving distance (see Lemma 5.3., Bubenik et al. (2023)).

**Definition 16.** Let  $M, N : \mathbb{R}^n \rightarrow \mathbf{Vec}$  be modules decomposing in the intervals  $\{J_j : j \in \mathcal{J}\}$  and  $\{K_k : k \in \mathcal{K}\}$ . The *p-Wasserstein distance* between  $M$  and  $N$  is defined as

$$d_{W_p}(M, N) = \inf_{\phi: \mathcal{I} \rightarrow \mathcal{K}} \left[ \sum_{\phi(i)=k} d_I(\mathbb{I}^{J_i}, \mathbb{I}^{K_k})^p + \sum_{j \in \mathcal{J} \setminus \mathcal{I}} d_I(\mathbb{I}^{J_j}, 0)^p + \sum_{k \in \mathcal{K} \setminus \phi(\mathcal{I})} d_I(0, \mathbb{I}^{K_k})^p \right]^{1/p}$$

where  $\phi$  ranges over all injections of subsets  $\mathcal{I} \subset \mathcal{J}$  into  $\mathcal{K}$ .

There have been other very recent approaches to extending Wasserstein metrics to multiparameter persistence (see Section 1.5. in Bjerkevik and Lesnick (2021) for further details) although their stability behavior and computability remains, at the time of research, an open question.

**Metrics on Rank Invariants.** The aim of our work is towards *computable* metrics on single and multiparameter persistence modules for computations and real data applications, even if they do not possess the theoretical properties of the interleaving distance. To this end, in the multiparameter setting, we study metrics directly defined on the rank invariant that do not rely on passing through the barcode decomposition. The *matching distance* (d’Amico et al., 2003, 2006, 2010) is a metric constructed via this approach.

**Definition 17.** For  $M, N \in \text{Vec}^{\mathbb{R}^n, \preceq}$  the *matching distance* between their rank invariants is defined as

$$d_{\text{match}}(\beta^M, \beta^N) := \sup_L \mathbf{m} \cdot d_B(\text{Bar}(M_L), \text{Bar}(N_L))$$

where  $L$  varies in the set of lines in  $\mathbb{R}^n$  such that  $\mathbf{m} = \min_{1 \leq i \leq n} m_i$  is strictly positive and  $M_L$  and  $N_L$  denote the single-parameter persistence modules obtained after restricting  $M$  and  $N$  to  $L$ .

The matching distance is known to be stable for rank invariants in multiparameter persistence (Cerri et al., 2013) for filtrations obtained as sublevel sets of a function  $f : X \rightarrow \mathbb{R}^n$  on  $X$  a triangulable space and with respect to the  $L^\infty$  distance between two possible filtering functions. In a more general setting, the matching distance is also known to be stable with respect to the interleaving distance (Landi, 2018), meaning that the matching distance between two p.f.d. multiparameter persistence modules is bounded above by the interleaving distance between the modules. In contrast to the interleaving distance, the matching distance is computable in polynomial time (Kerber et al., 2019).

A significant challenge, however, in using the matching distance in applications—especially in inferential statistics—despite its computability is that it does not induce a Hilbert structure on the space of rank invariants, which is often a condition needed in order to adapt functional data analytic methods (e.g., Crawford et al. (2020)). Thus, in this work, we focus on  $L^p$  metrics on rank invariants, which admit the required Hilbert structure when  $p = 2$ .

Rank invariants lie in the space of functions from  $\mathbb{R}^{2n+}$  to  $\mathbb{R}$  (Robins and Turner, 2016). By fixing a metric on the space  $\mathbb{R}^{2n+}$ , we can then define the  $L^p$  metric on this space of functions as follows:

$$d_{L^p}(f, g) := \left( \int_{\mathbb{R}^{2n+}} (f - g)^p d\omega \right)^{1/p},$$

where  $\omega$  is the measure on  $\mathbb{R}^{2n+}$  corresponding to the fixed metric. For notational simplicity, we write  $\|f - g\|_p = d_{L^p}(f, g)$ , keeping in mind that this metric comes from the  $L^p$  norm. There are many choices for the metric as well as for the measure  $\omega$ , though their choice should avoid that the pairwise distance between rank invariants be infinite. This happens, for example, when the metric is taken to be the Euclidean distance restricted to  $\mathbb{R}^{2n+}$ , which implies  $\omega$  is the Lebesgue measure. Here, two rank invariants have finite distance if and only if their infinite cycles have identical birth times.

*Remark 18.* In our work, such issues are circumvented by keeping in mind the goal of real data applications, where the posets over which we are defining our diagrams are always finite and in which the filtrations always end in a simplicial complex with trivial homology. This means that every cycle in the filtration is destroyed at some points, except for the 0-cycle representing the connected component of the space, which is always born at time 0. Thus, we can work with the Lebesgue measure without worrying about infinite distances between rank invariants: all bars in our barcodes will be finite, and therefore, every two rank functions will have finite pairwise distance, as desired.

### 3 Inferential Machine Learning with Rank Functions

In this section, we study the performance of rank functions and invariants in machine learning tasks on both real and simulated data. Specifically, we focus on *inferential* tasks—namely, classification, hypothesis testing, and prediction—in both the single and biparameter persistence settings.

**Using Persistent Homology in Data Analysis.** Persistent homology captured by persistence diagrams and barcodes fulfils the essential requirements for data analysis previously mentioned, namely interpretability (via the Structure Theorem) and stability (with various stability results available). Moreover, it is known to be a viable space for probability and statistics (Mileyko et al., 2011; Blumberg et al., 2014). Despite these desirable properties of persistence diagrams and barcodes, there remain challenges in implementing them in the full scope of statistical analysis. These challenges are largely due to its complicated geometry as an Alexandrov space with curvature bounded from below under the 2-Wasserstein distance, resulting in non-unique geodesics and Fréchet means (Turner et al., 2014).

There is a significant and growing literature on probabilistic aspects of persistent homology (see e.g., Adler et al. (2010); Chazal et al. (2015); Bobrowski and Kahle (2018)), while for statistical questions, there are, broadly speaking, two approaches to handling persistent homology of data, given the complex geometric structure of the space of persistence diagrams and barcodes. One approach entails developing data analytic methodology, such as machine learning algorithms and statistical models, to accommodate barcodes or persistence diagrams directly (e.g., Fasy et al. (2014); Reininghaus et al. (2015); Hofer et al. (2017)). The other approach entails vectorizing persistence to apply existing methods (e.g., Chazal et al. (2014); Bubenik (2015); Adams et al. (2017)).

In our work, we follow neither approach: we study rank functions and rank invariants as an alternative representation of persistent homology in order to benefit from FDA theory, which was developed to analyze data taking the form of functions, curves, and surfaces. Methods for FDA are well-established in statistics (see, e.g., Ramsay (2005, 2002) for a foundation to FDA techniques and applications) and many of them arise from extensions of methodologies from multivariate data analysis. Rank functions, being functions, are thus candidate data structures for persistent homology within framework of FDA. Equipped with the  $L^2$  metric as discussed above, the metric space of rank invariants  $(\mathcal{I}_n, L^2)$  admits a Hilbert structure and thus the theory of functional data analysis becomes amenable to persistent homology captured by rank functions.

We emphasize here that we are not modifying the output of persistent homology, as vectorization methods do to persistence diagrams or barcodes, since rank functions are equivalent to barcodes (see (2) above). Nor are we developing new methodology to accommodate persistent homology, as the existing field of FDA is directly applicable to persistent homology captured by rank functions.

*Remark 19.* We make a slight abuse of terminology in this section, contrasting Definitions 1 and 2, and simply refer to both rank functions and rank invariants as simply rank functions. Our reasoning for doing so is to emphasize the suitability of rank functions and rank invariants, as both functions, to FDA.

#### 3.1 Functional Support Vector Machine on Single-Parameter Rank Functions

Our first study is the performance of rank functions in the single-parameter persistence setting in classification. Specifically, we study the clinical application of discerning heart rate variability between healthy individuals and post-stroke (acute ischemic) patients using the *functional support vector machine* (FSVM) (Rossi et al., 2005).

Classical SVMs are supervised binary classification methods that seek to find boundaries between observations of two different categories in a maximizing manner. They benefit from the use of *kernels*, i.e., nonlinear mappings which project the data onto a higher dimensional space to give greater distinguishabil-

ity between the two categories. In what follows, let  $\{f_1, f_2, \dots, f_N\}$  be a collection of computed, centered, discretized rank functions with corresponding labels  $(y_i)_{i=1, \dots, N} \in \{-1, 1\}$  separating the two groups.

**Functional Data Analysis and High Dimensionality.** Functional data, where datasets are collections of functions, are inherently infinite dimensional, which means that the discrete realizations of the underlying surfaces or curves are high dimensional and can cause various problems such as overfitting.

However, FDA methodologies are generally insensitive to dimensionality; they circumvent the problem of high dimensionality in two ways: One way is via dimensionality reduction techniques, where projecting the data onto a smaller collection of orthogonal bases produces lower dimensional vectors that are robust to discretizations. The choice of basis function depends on the underlying functions; e.g., the Fourier basis functions can be used to approximate functions that exhibit cyclical properties, while wavelet basis functions can be used to approximate functions that exhibit fluctuations. Alternatively a data driven approach may be adopted, with one of the most commonly used techniques being *functional* PCA (FPCA) (Dauxois et al., 1982), which has previously been implemented on rank functions by Robins and Turner (2016). FPCA works on the principle of finding orthonormal basis functions and projecting onto a finite subset of them with the greatest variation.

The second way to circumvent this problem of high dimensionality is to ensure within the construction of the methodology that it is invariant to the choice of grid points for evaluation, such that as the number of grid points increases, convergence to an appropriate result is guaranteed by construction. This is known as the *refinement invariance principle* (Cox and Lee, 2008).

**Functional Support Vector Machine.** We adopt the *soft margin* approach to determine the boundary in our FSVM for rank functions for conventional reasons, as it is used in most computational packages. The aim is to find a boundary hyperplane separating the two labels that maximizes the margin encapsulating the boundary, giving some leeway for false classification. The boundary can be defined for some function  $\psi \in \mathcal{H}$ ,  $\mathcal{H}$  being a Hilbert space, and scalar  $b \in \mathbb{R}$  as  $\langle \psi, f_i \rangle + b = 0$ , such that

$$y_i(\langle \psi, f_i \rangle + b) \geq 1 - \zeta_i, \forall i = 1, \dots, n.$$

The margin is equal to  $\frac{2}{\|\psi\|}$  and the  $\zeta_i$ s are slack variables providing trade-offs between accuracy and overfitting. The optimization problem can be solved more easily through the dual formulation,

$$\max_{\alpha} \sum_{i=1}^n \alpha_i - \sum_{i=1}^n \sum_{j=1}^n \alpha_i \alpha_j y_i y_j \langle f_i, f_j \rangle \text{ s.t. } \sum_{i=1}^n \alpha_i y_i = 0, 0 \leq \alpha_i \leq C, \forall i = 1, \dots, n,$$

by sequential minimal optimization (Platt (1998)). To reconstruct the boundary, we compute  $\psi = \sum_{i=1}^n \alpha_i y_i f_i$  and  $b = \sum_{i=1}^n \alpha_i y_i \langle f_i, f \rangle - y$ , for any  $f$  and  $y$  lying on the margin. To predict the class for any new function,  $f_{N+1}$ , we simply compute  $\text{sgn}(\langle \psi, f_{N+1} \rangle + b)$ .

Practically, however, not all data are linearly separable, in which case, an approach is to project the data to higher dimensions where a clearer division between the two classes then becomes observable. This technique is referred to as the *kernel trick* (Boser et al., 1992). Let  $\phi$  be the projection, then we replace the inner product from the previous optimization problem by a kernel function, e.g.,  $\langle \phi(f), \phi(g) \rangle$ . Common kernels include the *polynomial* kernel (of order  $d$ ),  $K(f, g) = (\langle f, g \rangle + 1)^d$ , and the *Gaussian radial basis function* (GRBF) kernel,  $K(f, g) = \exp(-\gamma \|f - g\|^2)$  (Rossi et al., 2005). Their usage can be seen in a wide range of biomedical applications, for example, in the identification of PTSD patients based on resting state functional magnetic resonance imaging (fMRI) (Saba et al., 2022) and also in the classification of brain functions on electroencephalographic signals (Xie et al., 2008). In these two examples, the GRBF kernel has been seen to outperform other kernels and classifiers.

In this application, we study series of recorded beat-to-beat intervals (RR series) from a clinical study containing both a healthy cohort and a patient cohort of post acute ischemic stroke patients (Gąsecki et al. (2021), Narkiewicz et al. (2021)). We aim to discern differences in heart rate variability between the two groups using persistent homology rank functions.

**Data Description.** The dataset consists of 86 sequences of 512 RR series, beat-to-beat time intervals, extracted from electrocardiograms (ECGs) for two groups of people in a similar age category: one group of 46 healthy individuals used as control and one group of 40 patients who have recently experienced stroke episodes. Stroke patients generally show reduced heart rate variability compared with healthy individuals (Lees et al. (2018)). We linearly interpolated between the points in the RR series to construct continuous functions over time and construct a sublevel set filtration based on the height function in the positive  $y$ -direction. We compute the zero-dimensional persistent homology rank function for each individual’s RR series in the dataset. An example of how one RR series for a healthy individual was converted into a rank function is shown in Figure 2.

**Training the FSVM Classifier and Evaluating Performance.** On the set of rank functions computed from the data, we train functional SVM classifiers using the linear kernel, GRBF kernel, and polynomial kernels of three different degrees (2, 3, and 5). Since we are working with discretized functions, we consider both the rank functions as computed from the data, and transformed versions using dimension reduction. We experiment with both a set of data driven basis functions obtained from FPCA and a set of standard basis functions—the Haar wavelets. Haar wavelets, in particular, have also been used in other inferential tasks in persistent homology; Häberle et al. (2023) use them in persistent homology density estimation.

We evaluate the performance of the binary classifiers using two metrics: the accuracy and the area under the curve of the Receiver Operator Curve (AUC–ROC). The evaluation is carried out and averaged over ten iterations of five-fold cross-validation.

**Results.** The performance results of the FSVM classifier are summarized in Table 1. Overall, the FSVM classifiers with degree two and three polynomial kernels produce highest accuracy,  $> 80\%$ , compared to the performance of other kernels implemented and gave on average AUC–ROC values of over 0.8, indicating excellent discrimination between the two categories.

In general, linear kernels perform less well in discriminating between functions of the two categories, except when the dimensionality of the rank functions is reduced by projecting onto its principal component functions. In doing so, we considered only the first 30 principal component functions with the largest eigenvalues, which explains 95% of the variation. For the two transformations, working with lower dimensional vectors and polynomial kernels, we see similar, and slight improvements in accuracy and AUC–ROC of the classifiers than the original rank function.

Compared to non-persistence approaches, the optimized performance of the classifier using rank functions was on average better than the performance of standard heart rate variability frequency and time domain parameters, which only achieved an average AUC–ROC of 0.79 and 0.75 respectively (Graff et al., 2021) (compared to 0.842 for the classifier using degree two polynomial kernel and either transformation).

Another existing persistence-based approach to this clinical application has been proposed by Graff et al. (2021). This work uses a wide range of topological indices extracted from the persistent diagrams—some more typical, such as the total number of intervals, the sum of the lengths of all the persistent intervals, various mean and standard deviations; some less conventional, such as the *persistent entropy* (due to Atienza et al. (2020) and given by  $h(r) = \sum_{i=1}^n -\frac{\ell_i}{L} \log_2 \frac{\ell_i}{L}$ , where  $\ell_i$  is the length of an interval and  $L$  is the sum of the length of all intervals), *frac 5%*, *100*, *200* (the number of intervals whose lengths are shorter than the

threshold of 5% the length of the longest interval, 100ms, and 200ms), *signal-to-noise ratio* (which is the ratio of the sum of “signal” intervals over the sum of “noise” intervals, where the signal is considered to be the intervals longer than the threshold of 5% the length of the longest interval and those not passing this threshold are considered as “noise”). They introduce new geometric measures called the *topological triangle indices*, which are based on the triangular interpolation on the RR interval histograms classically used in heart rate variability analysis and work by constructing a triangle on the persistence diagram with one side lying on the diagonal, enclosing a set of points with a small percentage of outliers and such that the triangle is as compact as possible. From this, the extracted indices are the triangle width (length of side of the triangle on the diagonal), the triangle height (perpendicular from the diagonal), the triangle location ( $x$ -coordinate of the base of the triangle), and the triangle proportion (between the remaining two edges of the triangle). From these topological indices, it was shown that a combination of parameters, such as the triangle height, triangle location, total number of intervals and length sum was able to achieve 0.83 AUC performance. However, indeed, computing these indices is a much more involved process.

The performance we find using rank functions, as a direct and equivalent representation of persistent homology (as opposed to vectorized and manipulated) is on par and slightly improved over the topological indices approach of Graff et al. (2021), which achieved average AUC–ROCs of between 0.83 and 0.84.

### 3.2 Simulation Study for Biparameter Rank Functions

We now aim to study the inferential capabilities of rank functions in the setting of multiparameter persistent homology. Specifically, we conduct numerical experiments where we simulate data and compute their biparameter rank functions, on which we perform hypothesis testing—a fundamental task in inferential statistics. The goal is to identify the influence of noise on the data via persistence.

**Data Simulation.** We sample points from a circle of radius 2 and contaminate the data by introducing different types of noise and outliers to the samples, mimicking the types of influences that may be seen in real data. We study the following noise contaminations.

- **Noise 1:** Addition of a single outlier placed at the centre of the circle to points sampled from the circle.
- **Noise 2:** Gaussian noise with 0.01 variance applied to points sampled on the circle.
- **Noise 3:** Exponential noise with variance of 0.01 applied to the points sampled on the circle.
- **Noise 4:** Noise sampled from the power law distribution applied to the points sampled from the circle (the shape and scale parameters are chosen to be 3 and  $\frac{1}{5\sqrt{3}}$  respectively such that the variance is equal to 0.01).
- **Noise 5:** A combination of a single outlier at the centre of the circle and Gaussian noise perturbation (with 0.01 variance) applied to the points sampled from the circle.
- **Noise 6:** In addition to Noise 5, we include a small number of extreme outliers outside the circle which are constructed by applying a factor, uniformly sampled between 1.25 and 3, to the radii of the selected extreme points sampled on the circle.

The study of Noise 3 and Noise 4 is motivated by known results on topological “*crackle*” by Adler et al. (2014), who studied the homology of noise: moderate amounts of Gaussian noise introduced to a manifold do not significantly affect its homology, however, other types of noise (e.g., generated from the exponential or power law distributions) will tend to create artificial features that obscure the original homology. Note,

however, that their study takes place in the setting of single-parameter persistent homology while here, we are studying biparameter persistent homology. In addition, their study takes place over more complex manifolds and surfaces, while here, we work with samples from the circle in two dimensions.

The intuition for the study of Noise 6 is to introduce more extreme outliers to significantly affect the homology.

Figure 3 shows examples of the data plotted with the various types of noise above together with their corresponding persistence diagrams from Vietoris–Rips filtrations. Notice that we can identify by eye the subtle differences within the persistence diagrams introduced by the various noise and outliers; we can quantify these differences using the bottleneck or Wasserstein distances for persistence diagrams or  $L^2$  distance for the rank functions and invariants.

**Hypothesis Testing by Randomization.** The differences within a collection of sampled points can be quantified using loss functions; a common choice for loss function that we adapt in this study is the *mean squared error* loss.

**Definition 20.** For a collection of sampled data  $X_1, \dots, X_N$ , the *mean squared error* is given by

$$\text{MSE} = \frac{1}{N} \sum_{i=1}^N (X_i - \bar{X})^2,$$

where  $\bar{X} = \frac{1}{N} \sum_{i=1}^N X_i$ .

We use the loss function as the test statistic and apply a pairwise re-randomization type hypothesis test on collections of sampled data with and without noise and outliers to determine whether their computed persistent homology are significantly different to each other under the influence of noise. Under our null hypothesis, two collections of data are assumed to be generated by the same underlying process. Persistent homology here can be represented in a number of ways: either in the form of persistence diagrams or barcodes, or in the form of one or two-parameter rank functions. Specifically, we conduct the hypothesis test in the following metric spaces:  $(\mathcal{D}, d_B)$ ,  $(\mathcal{I}_1, L^2)$ ,  $(\mathcal{I}_2, L^2)$ .

The general procedure for a re-randomization test is as follows:

1. Given two sets of data and a chosen test statistic, we compute the test statistic (estimator of variation) on this original grouping,  $T$ ;
2. Then we permute the groups in a manner similar to resampling and recalculate the test statistic on the new grouping;
3. Repeating the previous step a large number of times, we obtain an approximation of the distribution of the test statistic under the null hypothesis ( $H_0$ ), with which we can evaluate the likelihood of acquiring our original test statistic ( $T$ ), generate an estimated  $p$ -value, and reason whether or not we should reject the assumption under the null hypothesis.

Here, we take the MSE—an estimator for the within-group variation—as the test statistic, since under  $H_0$  we hypothesize that the two sets of data are generated by the same mechanism and permuting the data randomly between the two groups should not lead to significantly more variation within each group. For two collections of computed rank functions  $\{f_{1,i}, f_{2,i}\}_{i=1,\dots,n}$ , the test statistic is of the form

$$L(f_{1,\cdot}, f_{2,\cdot}) = \sum_{k=1}^2 \frac{1}{n-1} \sum_{i=1}^n \|f_{k,i} - \bar{f}_k\|_2^2,$$

where  $\bar{f}_k$  is the pointwise mean. However, in the case of persistence diagrams, the mean is not easily computable as it is not unique (Turner et al., 2014); to bypass this issue, we use the following expression (Robinson and Turner, 2013):

$$L(X_1, X_2) = \sum_{k=1}^2 \frac{1}{2n(n-1)} \sum_{i=1}^n \sum_{j=1}^n W_p(X_{k,i}, X_{k,j})^q,$$

where  $W_p(\cdot, \cdot)$  is the  $p$ -Wasserstein distance and  $q \in [0, \infty)$ . This expression follows intuitively from the case of vectors where the estimate of the variance can be equivalently expressed as either  $\hat{\sigma}^2 = \frac{1}{n-1} \sum_{i=1}^n (x_i - \bar{x})^2$

or  $\hat{\sigma}^2 = \frac{1}{2n(n-1)} \sum_{i=1}^n \sum_{j=1}^n (x_i - x_j)^2$ . Note that the latter case does not require the computation of a unique mean.

For this simulation study we will restrict to only using the case where  $q = 1$ . Given the computation cost of computing each of the pairwise Wasserstein distances, computing the test statistic in terms of persistence diagrams is in general much more computationally expensive than computing the test statistic via the rank functions.

For each of the noise generation methods shown in Figures 3(b)–3(g), we simulated 100 samples and computed their respective persistent homology representations: persistence diagrams; single-parameter rank functions using the Vietoris–Rips filtration; and biparameter rank functions using the Degree–Rips bifiltration. We performed the re-randomization test on the collection of samples from the circle and the collection of samples from the circle with noise types given above and, using Monte Carlo methods over 5000 iterations, we generated an estimation of the approximate null distribution and an unbiased estimate for the  $p$ -value following the algorithm described by Robinson and Turner (2013).

Figures 4(a)–4(f) show the approximate null distributions of the test statistics (computed using persistence diagrams) from pairwise comparisons between the collection of circle samples and collections of circle samples with different types of noise and outliers as indicated in the captions.

**Results.** In both Figures 4(a)–4(f) and Figures 4(g)–4(l), we observe that the true values lie far to the left extreme of the null distributions, and, together with the  $p$ -values given in Table 2, indicate that the collection of samples from the circle are significantly different from the collections of samples influenced by noise and outliers. For these cases, the homology is computed from a single-parameter Vietoris–Rips filtration on the metric spaces  $(D, d_B)$  and  $(\mathcal{I}_1, L^2)$ , visually highlighting the weaker performance of the single-parameter Vietoris–Rips filtration when dealing with noise.

For Figures 4(m)–4(r), we considered instead the biparameter rank function summaries computed from the degree–Rips bifiltration (The RIVET Developers, 2020). We observe that for Figures 4(m)–4(q), the original test statistics lie roughly in agreement with the null distribution and give reasons to assume that the collections of noisy samples are sampled from the circle. When there are many outliers introduced into the samples as in Figure 4(r), the test concludes that the collections of samples are significantly different, as expected. Interestingly, if we choose our significance level of our hypothesis test to be 0.05, then this means that the the collection of samples with Gaussian noise can be considered to have the same homology as samples from the circle, whereas the collection of samples with exponential and power law noise cannot, which is in agreement with the findings by Adler et al. (2014).

*Remark 21.* The degree–Rips filtration is an easily computable, density-based bifiltration and a natural multiparameter extension to the standard Vietoris–Rips filtration in single-parameter persistence. Given a metric space, the degree–Rips complex of parameters  $(s, k)$ , where  $s > 0$  is a scale parameter and  $k \in \mathbb{N}$  is a threshold parameter, is the subcomplex of the Vietoris–Rips complex at scale  $s$ , constructed on points whose degree is at least  $k - 1$  in the 1-skeleton (Lesnick, 2015).

Recall that the Vietoris–Rips complex in a finite metric space  $(X, d_X)$  and for  $r \in \mathbb{R}_{\geq 0}$  is the simplicial complex with vertex set  $X$  where  $\{x_0, x_1, \dots, x_k\}$  spans a  $k$ -simplex if and only if the diameter  $d_X(x_i, x_j) \leq r$  for all  $0 \leq i, j \leq k$ .

**Numerical Comparison of Stability Performance.** To numerically compare the stability of the various representations of persistent homology discussed above (i.e.,  $(\mathcal{D}, d_B)$ ,  $(\mathcal{D}, W_2)$ ,  $(\mathcal{I}_1, L^2)$ ,  $(\mathcal{I}_2, L^2)$ ), we generated a series of pairs of 100 samples, each from the circle and from the circle with added Gaussian noise where we increase the standard deviation of the noise from 0 to 0.25 in 0.01 increments. Then, for each pair of 100 samples, we computed their persistence diagrams, single-parameter rank functions (using Vietoris–Rips filtration), and the biparameter rank functions (using degree–Rips filtration), and carry out re-randomization testing as described above using both the 2-Wasserstein and bottleneck distance for the persistence diagrams, and the  $L^2$  distance for the rank functions. Figure 5 shows the mean  $p$ -values ( $\pm 1$  s.d.) of the tests for increasing Gaussian noise over 10 iterations. Here, we can see that the resistance to noise for the single-parameter rank functions is in between the resistance to noise for the persistence diagrams using  $p$ -Wasserstein and bottleneck distances, with the  $p$ -Wasserstein distance having a lower susceptibility to noise. The biparameter rank functions, on the other hand, as we would expect, have greater resistance to noise and succumb to the noise only after a much larger amount is introduced.

### 3.3 Application of Biparameter Rank Functions in Lung Tumor Classification

We now demonstrate the inferential ability of the biparameter rank functions using nonparametric supervised learning methods on real data. The application focus is to predict lung tumor malignancies from computed tomography (CT) images, which has been studied previously by Vandaele et al. (2023) using single-parameter topological summary statistics. Here, we aim to show that using biparameter persistent homology captures additional distinguishing features of the tumor morphology, both on a local and global scale, which, together with the rank functions, leads to improved classification.

**Data Description.** We study images from the Lung Image Database Consortium (LIDC), which is freely available from The Cancer Imaging Archive (TCIA) (Armato III et al. (2011), Armato III et al. (2015)). From the LIDC data, we extract a subgroup of 115 chest CT scans, complete with annotations and masks, consisting of those that have been diagnosed as benign, primary malignant, and metastatic malignant. The total number of scans within each of these subcategories are 29, 41, and 45, respectively.

Following the approach in Vandaele et al. (2023), we convert the collection of CT scan images and masks into 3D point clouds of landmarks on the tumor surfaces using sampling, as shown in Figure 6. On the resulting point clouds, we compute the biparameter rank function using the degree–Rips filtration or the Vietoris–Rips filtration combined with the  $x$ ,  $y$ , or  $z$  (also taken to be height) coordinates as the second filtration, building up the tumor region in these directions. Using the bifiltration captures prominent features as they develop on the tumor surface.

**Classification.** We utilize the following two supervised classification methods:

- **$k$ -Nearest Neighbors:** The  $k$ -nearest neighbors algorithm (Cover and Hart, 1967) is a fundamental classification technique for both multivariate data and functional data, where the decision for a new datum is made based on majority vote of its  $k$ -closest neighbors. The method is adaptable to different metric spaces since the proximity can be measured using various metrics; the method has been studied in persistence settings by Marchese et al. (2017); Cao et al. (2022). Here, we work in  $(\mathcal{I}_2, L^2)$ .
- **Functional Maximum Depth** (López-Pintado and Romo, 2009): This method uses an extended notion of *depth* on functional data to classify curves and surfaces.

For a collection of functions,  $f_1(x), \dots, f_n(x)$ ,  $x \in \mathcal{X}$ , where  $\mathcal{X}$  is the domain for the class of functions (in the case of rank functions, it is the space of the parameters), we define a *band* as the region or hyperspace bounded by an upper and lower function as follows:

$$B(f_1, \dots, f_n) = \{(x, y) : x \in \mathcal{X}, \min_{i=1, \dots, n} f_i(x) \leq y \leq \max_{i=1, \dots, n} f_i(x)\}.$$

The *band depth*  $BD$  is the total number of times that  $f$  lies within the band formed by a subcollection of the functions,

$$BD_{n,J}(f) := \sum_{j=2}^J BD_n^{(j)}(f)$$

for a fixed value  $J$ , where  $2 \leq J \leq n$  and

$$BD_n^{(j)}(f) = \binom{n}{j}^{-1} \sum_{1 \leq i_1 < i_2 < \dots < i_j \leq n} \mathbb{1}_{Bd(f)}, \quad (4)$$

where  $\mathbb{1}_{Bd(f)}$  is the indicator function of the set  $Bd(f) := \{G(f) \subseteq B(f_{i_1}, f_{i_2}, \dots, f_{i_j})\}$  for  $G(f) = \{(x, f(x)) : x \in \mathcal{X}\}$ . For our application, we use a modified band depth,  $MBD$ , where instead of using a strict indicator function in (4), we consider the proportion of the hyperspace for which that the function  $f$  lies within the band:

$$MBD_n^{(j)}(f) = \binom{n}{j}^{-1} \sum_{1 \leq i_1 < i_2 < \dots < i_j \leq n} \omega(A(f; f_{i_1}, f_{i_2}, \dots, f_{i_j})) / \omega(\mathcal{X}), \quad (5)$$

where  $\omega$  is a Lebesgue measure on  $\mathcal{X}$  and  $A(f; f_{i_1}, f_{i_2}, \dots, f_{i_j}) \equiv \{x \in \mathcal{X} : \min_{r=i_1, \dots, i_j} f_r(x) \leq f(x) \leq \max_{r=i_1, \dots, i_j} f_r(x)\}$ . Thus, for given classes of functions and a new function  $f$ , the class to which  $f$  will be assigned is the one which maximizes the modified band depth (5).

In the dataset we study, the true diagnosis (benign, primary malignant, metastatic malignant) is given for each of the tumor images. A natural classification question that arises is whether we can use the topological summaries as predictors to determine whether a primary tumor is benign or malignant. We train the classifiers on the biparameter rank functions computed from the whole dataset. Taking a 75/25 split of the data for training and testing and averaging over 50 iterations, we obtain the results in Table 3. Furthermore, 24 of the 29 CT scans of benign tumors and 17 of the 41 CT scans of malignant tumors were taken with added contrast material. Refining to this smaller set, we see further improvements in the predictive accuracies reported in Table 4.

**Results.** Without added contrast, our results show that by training a modified maximum depth ( $MBD$ ) classifier, we attain an optimal accuracy and AUC–ROC of 70.8 and 72.0 with the degree–Rips filtration. Overall the performances of  $MBD$  classifiers trained on the different bifiltrations are better than the performance of  $k$ -NN classifiers and also the optimized model in Vandaele et al. (2023) which achieved an AUC–ROC of 67.7 on this dataset.

Moreover, comparing the performance on the subset of data with added contrast material, we find again that both classifiers achieved better AUC–ROC with the  $x$ -Rips and  $y$ -Rips filtrations than the optimal model in Vandaele et al. (2023) which had an AUC–ROC of 78.0 on average. In fact, the average AUC–ROC for the best  $k$ -NN classifier based on  $h$ -Rips filtration was 83.0. Therefore, indeed we find that the additional information captured by the bifiltration leads to better predictions.

## 4 Computable Stability of Rank Functions and Rank Invariants

We now turn to validating the experimental results achieved by providing several stability guarantees of rank functions and rank invariants. We focus on the  $L^p$  metric, as opposed to Skraba and Turner (2021), who study the weighted version,

$$\|f - g\|_p^w = \left( \int_{\mathbb{R}^{2+}} |f - g|^p \phi(x - y) dx dy \right)^{1/p}. \quad (6)$$

The weight function  $\phi(\cdot)$  inside the integral satisfies  $\int_{\mathbb{R}} \phi(t) < \infty$ . In particular, they choose  $\phi(t) = e^{-t}$  and obtain the following stability result as a Corollary from Theorem 11.

**Corollary 22** (Skraba and Turner (2021)). *Rank functions with the  $L^q$  weighted metric (6) are 1-Lipschitz with respect to the  $p$ -Wasserstein distance between diagrams if and only if  $p = q = 1$ .*

The presence of the weight function in (6) ensures finiteness of distances between rank functions (Lemma 2.1., Robins and Turner, 2016), which in turn ensures that any finite set of rank functions lies in an affine space allowing for a notion of an inner product, and thus justifies the use of FDA methods such as the FPCA using rank functions proposed by Robins and Turner (2016). As mentioned previously in Remark 18, here, we guarantee finiteness of  $L^p$  distances between pairwise rank functions using the fact that in our setting, there is only one essential component in homological degree 0 which is always born in the first step of the filtration (i.e., “at time zero”), so there are no essential cycles with different birth times that would cause infinite  $L^p$  distances between rank functions.

The introduction of the weight also fundamentally changes the expressions in the computations involving the metric. As a result, the proof of Corollary 22 by Skraba and Turner (2021) does not apply and cannot be replicated in our setting. Moreover, it does not extend to the multiparameter setting—a goal that we achieve further on in Section 4.2. For these reasons, although relevant, the study of rank function stability by Skraba and Turner (2021) strictly differs to ours.

### 4.1 Stability of Rank Functions

In the setting of single-parameter persistent homology, we establish two stability results for the  $L^p$  metrics on rank functions compared to the bottleneck distance and 1-Wasserstein distance.

**Stability under the Bottleneck Distance.** The most straightforward way to achieve stability for rank functions is to restrict away from the diagonal, which is known to complicate the metric geometry of the space of persistence diagrams (Turner et al., 2014; Cao and Monod, 2022b). To do this, we introduce a truncation of the rank function that will allow us to compare its sensitivity to noise to that of the bottleneck distance.

**Definition 23.** For any rank function  $\beta$  and any  $\delta > 0$ , we define the  $\delta$ -truncated rank function as

$$\beta_\delta := \beta \cdot \mathbb{1}_{\mathbb{R}_\delta^{2+}}$$

where  $\mathbb{1}_{\mathbb{R}_\delta^{2+}}$  is the indicator function of the set  $\mathbb{R}_\delta^{2+} := \{(x, y) \in \mathbb{R}^{2+} : y > x + \delta\}$ .

In other words, the truncated rank function is just the rank function excluding a strip of width  $\delta > 0$  above the diagonal  $\partial$  (see Definition 3). The truncated rank function locally satisfies a Hölder inequality for the  $L^p$  norm with respect to the bottleneck distance on persistence diagrams.

**Proposition 24** (Bottleneck stability for truncated rank functions). *Let  $1 \leq p < \infty$  and  $M$  be a  $p.f.d.$  persistence module with finite intervals in its barcode decomposition. For every  $\delta > 0$ , there exist  $1 \geq \eta > 0$  and  $K_{M,p} > 0$  such that any persistence module  $N$  satisfying*

$$d_B(\text{Dgm}(M), \text{Dgm}(N)) < \eta$$

also satisfies

$$\|\beta_\delta^M - \beta_\delta^N\|_p \leq K_{M,p} \cdot d_B(\text{Dgm}(M), \text{Dgm}(N))^{1/p}. \quad (7)$$

In other words, the map  $(\mathcal{D}, d_B) \rightarrow (\mathcal{I}_1, L^p)$  which sends each persistence diagram to its correspondent rank function is locally Hölder with exponent  $1/p$ .

*Proof.* Let  $M = \bigoplus_{j \in J} \mathbb{I}[b_j, d_j]$  be the interval decomposition of  $M$  with  $J$  finite and call  $\delta_j = b_j - d_j$  for  $j \in J$ . Take an arbitrary  $\delta > 0$  and

$$\eta < \min \left( \left\{ \frac{\delta_j}{2} : j \in J \right\} \cup \left\{ \frac{\delta}{2} \right\} \cup \{1\} \right);$$

let  $N$  be a persistence module such that  $d_B(\text{Dgm}(M), \text{Dgm}(N)) < \eta$ .

Denote by  $h$  the bijection between  $\text{Dgm}(M)$  and  $\text{Dgm}(N)$  induced by the bottleneck distance and call  $(b'_j, d'_j) := h(b_j, d_j)$  for all  $j \in J$ . Since  $\eta < \delta_j/2$  for all  $j \in J$ , every point outside of the diagonal from  $\text{Dgm}(M)$  gets matched to a point outside of the diagonal in  $\text{Dgm}(N)$ . Also, since  $\eta < \delta/2$ , the remaining points from  $\text{Dgm}(N)$  that get matched to the diagonal lie in the set  $\{(x, y) \in \mathbb{R}^{2+} : y < x + \delta\}$ .

For  $j \in J$  we define the sets

$$\begin{aligned} A_j &:= \{(x, y) \in \mathbb{R}^{2+} : b_j \leq x \leq y \leq d_j\}, \\ B_j &:= \{(x, y) \in \mathbb{R}^{2+} : b'_j \leq x \leq y \leq d'_j\}, \\ D_j &:= A_j \Delta B_j = (A_j \cup B_j) \setminus (A_j \cap B_j), \end{aligned} \quad (8)$$

where  $\Delta$  denotes the symmetric difference (see Figure 7 for some illustrative examples of  $D_j$ ). Notice that for  $(x, y) \in D_j^c$

$$\beta^{\mathbb{I}[b_j, d_j]}(x, y) = \beta^{\mathbb{I}[b'_j, d'_j]}(x, y) \quad (9)$$

and that these rank functions differ by one for  $(x, y) \in D_j$ .

Set

$$D := \bigcap_{j \in J} D_j^c.$$

If  $(x, y) \in D$  then  $\beta^M(x, y) = \beta^N(x, y)$ . Indeed, if  $y \leq x + \delta$ , we directly obtain  $\beta_\delta^M(x, y) = \beta_\delta^N(x, y) = 0$  and if  $y > x + \delta$ , we have

$$\begin{aligned} \beta_\delta^M(x, y) &= \beta^M(x, y) \\ &= \beta^N(x, y) \\ &= \beta_\delta^N(x, y) \end{aligned} \quad (10)$$

where (10) holds from the additivity of the rank functions, since in this region there is a bijection between the points in both diagrams and the points in  $\text{Dgm}(N)$  matched to the diagonal are not counted.

Now, we bound the Lebesgue measure of  $D^c$  from above. To do so, we define

$$R := \max(\{d_j - b_j : j \in J\}).$$

Observe that  $R < \infty$  since all the intervals in the barcode decomposition of  $M$  are finite.

Let us fix some  $j \in J$ . The rectangles depicted in Figure 7 both have one side of length

$$\max(d'_j, d_j) - \min(b_j, b'_j) = \begin{cases} d_j - b'_j \leq d_j - b_j + \|(b_j, d_j) - (b'_j, d'_j)\|_\infty & \text{(corresponding to Figure 7(a)),} \\ d'_j - b_j \leq d_j - b_j + \|(b_j, d_j) - (b'_j, d'_j)\|_\infty & \text{(analogous to the previous case),} \\ d'_j - b'_j \leq d_j - b_j + 2\|(b_j, d_j) - (b'_j, d'_j)\|_\infty & \text{(corresponding to Figure 7(b)),} \\ d_j - b_j & \text{(corresponding to Figure 7(c)).} \end{cases}$$

The other side of both rectangles is bounded by  $\|(b_j, d_j) - (b'_j, d'_j)\|_\infty$ . Observe that this is also a bound for the lengths of the sides of the rectangle in the intersection.

In case 7(c), by adding the Lebesgue measure of the rectangles, we get

$$\omega(D_j) \leq 2(d_j - b_j) \|(b_j, d_j) - (b'_j, d'_j)\|_\infty$$

where  $\omega(\cdot)$  denotes the Lebesgue measure. In cases 7(a) and 7(b), adding the Lebesgue measure of the rectangles and triangles that decompose the figures, we obtain

$$\begin{aligned} \omega(D_j) &\leq 2(d_j - b_j) \|(b_j, d_j) - (b'_j, d'_j)\|_\infty + 2 \|(b_j, d_j) - (b'_j, d'_j)\|_\infty^2 \\ &\leq 2(d_j - b_j + 1) \|(b_j, d_j) - (b'_j, d'_j)\|_\infty \end{aligned}$$

where we have used that  $\|(b_j, d_j) - (b'_j, d'_j)\|_\infty \leq 1$  in the last inequality.

Putting both bounds together, we obtain that for any  $j \in J$ :

$$\omega(D_j) \leq 2(d_j - b_j + 1) \|(b_j, d_j) - (b'_j, d'_j)\|_\infty \quad (11)$$

and thus, since  $D^c = \bigcup_{j \in J} D_j$ , we conclude

$$\omega(D^c) \leq 2(R+1)|J| \cdot d_B(\text{Dgm}(M), \text{Dgm}(N)). \quad (12)$$

Recall that for a point  $(x, y) \in D_j$  with  $j \in J$ , the value of the rank functions  $\beta^{\lfloor b_j, d_j \rfloor}(x, y)$  and  $\beta^{\lfloor b'_j, d'_j \rfloor}(x, y)$  differs by one. Since  $(x, y)$  can belong to at most  $|J|$  spaces,  $D_j$ , at the same time, we conclude that for all  $(x, y) \in D^c$ , we have  $|\beta_\delta^M(x, y) - \beta_\delta^N(x, y)| \leq |J|$ . We can now obtain the bound in (7):

$$\begin{aligned} \|\beta_\delta^M - \beta_\delta^N\|_p &= \left( \int_{D^c} |\beta_\delta^M - \beta_\delta^N|^p d\omega \right)^{1/p} \\ &\leq |J| \omega(D^c)^{1/p} \\ &\leq (2R+2)^{1/p} |J|^{(p+1)/p} \cdot d_B(\text{Dgm}(M), \text{Dgm}(N))^{1/p}. \end{aligned} \quad (13)$$

□

Notice that we can always obtain a bound similar to that in (7) where the constant depends on both persistence modules  $M$  and  $N$  as follows: Let  $R$  be the maximum between the lifetimes of the bars in the barcodes of  $M$  and  $N$ , so that  $\omega(D_j) \leq 2R \cdot d_B(\text{Dgm}(M), \text{Dgm}(N))$  and use this bound in the last sequence of inequalities of the previous proof. Proposition 24 refines this approach by obtaining a constant that only depends on the persistence module  $M$ .

Nevertheless, we point out that an important limitation of Proposition 24 is that it discards the points close to the diagonal, although it sheds light on the behavior of rank functions in discrete settings. The bounds in (11) and (12) will be useful in our next derivations.

A natural question is whether it is possible to achieve a bound such as in (11), but with the following dependence with respect to the bottleneck distance

$$\omega(D_j) \leq C(b_j, d_j) \cdot d_B(\text{Dgm}(M), \text{Dgm}(N))^p$$

for some values  $p \geq 2$ , implying a Lipschitz stability condition (notice that for  $p = 1$  Proposition 24 is actually a Lipschitz condition). In a similar vein to Corollary 22 by Skraba and Turner (2021), the answer to this question is negative, as we show next.

**Proposition 25.** *Take  $\mathbb{I}[b, d]$  and  $C(b, d) = 2(d - b + 1) > 0$  such that*

$$\omega(D) \leq C(b, d) \cdot \|(b, d) - (b', d')\|_\infty$$

*for some other interval module  $\mathbb{I}[b', d']$ , with  $\|(b, d) - (b', d')\|_\infty < 1$  and  $D \subset \mathbb{R}^{2+}$  as defined in (8) (see also (11)). Then*

$$\omega(D) > C(b, d) \cdot \|(b, d) - (b', d')\|_\infty^p$$

*for every  $p \geq 2$ .*

*Proof.* Let  $\epsilon > 0$  and consider  $\mathbb{I}_\epsilon := \mathbb{I}[b - \epsilon, d + \epsilon]$  so that  $\|(b, d) - (b - \epsilon, d + \epsilon)\|_\infty = \epsilon$ . In this case we are in a situation similar to the one depicted in Figure 7(b). Define

$$D_\epsilon := \{(x, y) \in \mathbb{R}^{2+} : b \leq x \leq y \leq d\} \Delta \{(x, y) \in \mathbb{R}^{2+} : b - \epsilon \leq x \leq y \leq d + \epsilon\}.$$

For this domain, we exactly have

$$\omega(D_\epsilon) = 2(d - b)\epsilon + 2\epsilon^2$$

and taking  $0 < \epsilon < 1$ , we get

$$\omega(D_\epsilon) = 2(d - b)\epsilon + 2\epsilon^2 > 2(d - b + 1) \cdot \epsilon^p = C(b, d) \cdot \epsilon^p$$

for every  $p \geq 2$ .

Now, for every other interval module  $\mathbb{I}[b', d']$  with  $\|(b, d) - (b', d')\|_\infty < 1$ , we can just consider the previous case with  $\epsilon = \min(|b' - b|, |d' - d|) < 1$ , so that  $D_\epsilon \subset D$  (as defined in (8)) and thus  $\omega(D_\epsilon) \leq \omega(D)$ , concluding the proof.  $\square$

**Stability under the 1-Wasserstein distance.** The limitation of Proposition 24 is that it holds only for points away from the diagonal, which highlights the differences in sensitivity to noise between the  $L^p$  norms on rank functions and the bottleneck distance on persistence diagrams. This observation was already made by Landi and Frosini (1997) and led them to instead focus on developing new pseudometrics better suited to establishing stability.

In contrast, our strategy is to maintain focus on the  $L^p$  distance—and more specifically, to the case where  $p = 2$ —because they are computationally tractable and they provide the Hilbert space structure to space of rank functions needed to implement the FDA applications seen in Section 3. Moreover, as we will now establish, they satisfy a stability property with respect to the 1-Wasserstein distance for persistence diagrams. As mentioned above in Section 2.3, stability properties of the Wasserstein metric on persistence diagrams were not studied in detail until very recently, which limited their applicability as upper bounds in stability studies. However, the Cellular Wasserstein Stability Theorem (Theorem 11) by Skraba and Turner (2021) now ensures that stability may be concluded from this approach, which motivates our search for a stability result under this metric.

**Theorem 26** (1-Wasserstein stability for rank functions). *Let  $p = 1, 2$ ; and  $M$  be a p.f.d. persistence module with finite intervals in its barcode decomposition. Then there exists a constant  $C_{M,p} > 0$  such that for any other p.f.d. persistence module  $N$  satisfying  $W_1(\text{Dgm}(M), \text{Dgm}(N)) \leq 1$ , we have*

$$\|\beta^M - \beta^N\|_p \leq C_{M,p} \cdot W_1(\text{Dgm}(M), \text{Dgm}(N))^{1/p}. \quad (14)$$

*In other words, the map  $(\mathcal{D}, W_1) \rightarrow (\mathcal{I}_1, L^1)$  which sends a persistence diagram to its corresponding rank function is locally Lipschitz, and the same map between the spaces  $(\mathcal{D}, W_1) \rightarrow (\mathcal{I}_1, L^2)$  is locally Hölder with exponent  $1/2$ .*

*Proof.* We write  $M = \bigoplus_{j \in J} \mathbb{I}[b_j, d_j]$  for the interval decomposition of  $M$ , with  $J$  finite and consider  $N$  a p.f.d. persistence module over  $\mathbb{R}$  such that  $W_1(\text{Dgm}(M), \text{Dgm}(N)) \leq 1$ . Let  $h$  be the bijection between  $\text{Dgm}(M)$  and  $\text{Dgm}(N)$  induced by the 1-Wasserstein distance. We extend  $J$  to  $J' \supseteq J$  such that  $N = \bigoplus_{j \in J'} \mathbb{I}[b'_j, d'_j]$  and  $M = \bigoplus_{j \in J'} \mathbb{I}[b_j, d_j]$  by adding intervals corresponding to points on the diagonal of  $\text{Dgm}(M)$  in order to have that  $h(b_j, d_j) = (b'_j, d'_j)$  for all  $j \in J'$ . For  $j \in J$ , define the set  $D_j$  as in (8).

The rank function is an additive function: when  $M$  decomposes as above, its rank function follows the decomposition

$$\beta^M = \sum_{j \in J'} \beta^{\mathbb{I}[b_j, d_j]}.$$

This gives the following sequence of inequalities

$$\begin{aligned} \|\beta^M - \beta^N\|_p &= \left\| \sum_{j \in J'} \beta^{\mathbb{I}[b_j, d_j]} - \beta^{\mathbb{I}[b'_j, d'_j]} \right\|_p \leq \left\| \sum_{j \in J} \beta^{\mathbb{I}[b_j, d_j]} - \beta^{\mathbb{I}[b'_j, d'_j]} \right\|_p + \left\| \sum_{j \in J' \setminus J} 0 - \beta^{\mathbb{I}[b'_j, d'_j]} \right\|_p \\ &\leq \sum_{j \in J} \left\| \beta^{\mathbb{I}[b_j, d_j]} - \beta^{\mathbb{I}[b'_j, d'_j]} \right\|_p + \sum_{j \in J' \setminus J} \left\| \beta^{\mathbb{I}[b'_j, d'_j]} \right\|_p. \end{aligned}$$

As seen in the proof of Proposition 24, for  $j \in J$ , we have  $\beta^{\mathbb{I}[b_j, d_j]} = \beta^{\mathbb{I}[b'_j, d'_j]}$  in  $D_j^c$ , and in  $D_j$  they differ by at most 1. This gives the bound

$$\left\| \beta^{\mathbb{I}[b_j, d_j]} - \beta^{\mathbb{I}[b'_j, d'_j]} \right\|_p \leq \omega(D_j)^{1/p}.$$

Notice also that the  $L^p$  norm of  $\beta^{\mathbb{I}[b'_j, d'_j]}$  for  $j \in J' \setminus J$  equals the  $p^{\text{th}}$ -root of the area of the triangle with vertices at  $(b'_j, d'_j)$ ,  $(b'_j, b'_j)$ , and  $(d'_j, d'_j)$ , which is equal to  $\frac{1}{2}|d'_j - b'_j|^2$ . For  $p = 1$  we can obtain the Lipschitz condition as follows

$$\begin{aligned} \|\beta^M - \beta^N\|_1 &\leq \sum_{j \in J} \omega(D_j) + \sum_{j \in J' \setminus J} \frac{1}{2}|d'_j - b'_j|^2 \\ &\leq \sum_{j \in J} \omega(D_j) + \sum_{j \in J' \setminus J} |d'_j - b'_j| \end{aligned} \tag{15}$$

$$\leq 2(R+1) \sum_{j \in J} \|(b'_j, d'_j) - (b_j, d_j)\|_\infty + \sum_{j \in J' \setminus J} |d'_j - b'_j| \tag{16}$$

$$\leq 2(R+1) \sum_{j \in J} (|b_j - b'_j| + |d_j - d'_j|) + \sum_{j \in J' \setminus J} |d'_j - b'_j|$$

$$\leq 2(R+2) \cdot W_1(\text{Dgm}(M), \text{Dgm}(N))$$

where in (17) we use that  $W_1(\text{Dgm}(M), \text{Dgm}(N)) \leq 1$  implies that  $\frac{|d'_j - b'_j|}{2} \leq 1$  for  $j \in J' \setminus J$  and in (16) we have used the bound in (11).

For the case where  $p = 2$ , applying the Cauchy-Schwarz inequality we get

$$\sum_{j \in J} \omega(D_j)^{1/2} \leq \left( |J| \sum_{j \in J} \omega(D_j) \right)^{1/2},$$

thus, we obtain

$$\|\beta^M - \beta^N\|_2 \leq (2(R+1)|J|)^{1/2} \left( \sum_{j \in J} \|(b'_j, d'_j) - (b_j, d_j)\|_\infty \right)^{1/2} + \frac{1}{\sqrt{2}} \sum_{j \in J' \setminus J} |d'_j - b'_j| \quad (17)$$

$$\leq \max \left\{ (2(R+1)|J|)^{1/2}, \frac{1}{\sqrt{2}} \right\} \cdot \left( W_1(\text{Dgm}(M), \text{Dgm}(N))^{1/2} + W_1(\text{Dgm}(M), \text{Dgm}(N)) \right) \quad (18)$$

$$\leq \max \left\{ (2(R+1)|J|)^{1/2}, \frac{1}{\sqrt{2}} \right\} \cdot W_1(\text{Dgm}(M), \text{Dgm}(N))^{1/2} \quad (19)$$

where in (17) we take the root and use the bound in (11); and in (19), we use that  $W_1(\text{Dgm}(M), \text{Dgm}(N)) \leq 1$ .  $\square$

Theorem 26 provides a stronger theoretical guarantee than Proposition 24, not only because it also covers the diagonal, but also because the constant  $C_{M,1}$  in (14) is smaller than the constant  $K_M$  in (7): the latter depends on the number of points in the persistence diagram of  $M$  whereas the former only depends on  $R$ , the difference between the maximal death and minimal birth in  $M$ . For  $C_{M,2}$  we maintain a dependence on the number of points in the diagram of  $M$ , but it still provides a tighter bound.

## 4.2 Computable Stability of Rank Invariants

We now study the computable stability of rank invariants. We begin by extending ideas from the single-parameter setting to study the stability of  $L^p$  metrics on rank invariants for rectangle decomposable modules. As mentioned above, the combinatorial nature of this metric makes it in principle a computationally feasible distance and thus relevant to our work.

**Stability of Rectangle Decomposable Rank Invariants.** We establish the following stability result for  $L^p$  distances on rank invariants and the 1-Wasserstein distance on rectangle decomposable multiparameter persistence modules (see Definition 16).

**Proposition 27.** *Let  $M$  and  $N$  be rectangle decomposable  $\mathbb{R}^n$ -persistence modules. Then, for  $p = 1, 2$  there exist  $c_{M,N,p,n} > 0$  such that*

$$\|\beta^M - \beta^N\|_p \leq c_{M,N,p,n} \cdot d_{W_p}(M, N)^{1/p}.$$

To prove this result, we need the following lemma which treats the case when both modules are interval modules.

**Lemma 28.** *Let  $U$  and  $V$  be two rectangles in  $\mathbb{R}^n$  and  $C > 0$  be the maximum over the lengths of the intervals defining  $U$ . If  $M = \mathbb{I}^U$  and  $N = \mathbb{I}^V$  are  $\epsilon$ -interleaved then there exists some  $c_{M,n} > 0$  such that*

$$\|\beta^M - \beta^N\|_p \leq (c_{M,n} \cdot \epsilon)^{1/p}$$

for all  $1 \leq p < \infty$ .

*Proof.* First, notice that for an interval module, i.e.  $\mathbb{I}^I$  where  $I$  is an interval of  $\mathbb{R}^n$ ; we get  $\beta^{\mathbb{I}^I} = \mathbf{1}_{\mathbb{R}^{2n} \cap I^2}$ . That way, similar to the single-parameter case, we have that

$$\|\beta^M - \beta^N\|_p = \omega(\mathbb{R}^{2n} \cap (U^2 \Delta V^2))^{1/p} \quad (20)$$

where  $\Delta$  denotes the symmetric difference,  $U^2 \Delta V^2 = (U^2 \setminus V^2) \cup (V^2 \setminus U^2)$ . The goal now is bounding this measure.

First, notice that from the definition of the  $\epsilon$ -interleaving (see Definition 12), we have that if  $C'$  is the maximum length of the intervals defining  $V$  then we must have

$$C' \leq C + 2\epsilon. \quad (21)$$

Call  $\vec{\epsilon} := \epsilon(1, \dots, 1)$ . Since  $M$  and  $N$  are  $\epsilon$ -interleaved, we have the commutative diagram,

$$\begin{array}{ccc} M(x - \vec{\epsilon}) & \xrightarrow{\quad\quad\quad} & M(y + \vec{\epsilon}) \\ & \searrow & \nearrow \\ & N(x) & \xrightarrow{\quad\quad\quad} & N(y) \end{array} \quad (22)$$

implying that the rank of the map  $N(x \leq y)$  is larger than the rank of  $M(x - \vec{\epsilon} \leq y + \vec{\epsilon})$ , i.e.,  $\beta^N(x, y) \geq \beta^M(x - \vec{\epsilon}, y + \vec{\epsilon})$ , or equivalently  $\mathbb{1}_{\mathbb{R}^{2n+} \cap V^2}(x, y) \geq \mathbb{1}_{\mathbb{R}^{2n+} \cap U^2}(x - \vec{\epsilon}, y + \vec{\epsilon})$ . From this, we conclude that for  $(x, y) \in \mathbb{R}^{2n+}$  such that  $(x - \vec{\epsilon}, y + \vec{\epsilon}) \in U^2$ , we have  $(x, y) \in V^2$ , or equivalently,

$$\mathbb{R}^{2n+} \cap (U + \vec{\epsilon} \times U - \vec{\epsilon}) \subseteq \mathbb{R}^{2n+} \cap V^2.$$

Therefore,

$$\begin{aligned} \mathbb{R}^{2n+} \cap (U^2 \setminus V^2) &\subseteq \mathbb{R}^{2n+} \cap (U^2 \setminus (U + \vec{\epsilon} \times U - \vec{\epsilon})) \\ &\subseteq [(U \setminus U + \vec{\epsilon}) \times U] \cup [U \times (U \setminus U - \vec{\epsilon})]. \end{aligned}$$

$U$  is a rectangle, so  $U = U_1 \times U_2 \times \dots \times U_n$ , with  $U_i$  intervals of length at most  $C > 0$ . Thus, we have

$$U \setminus (U + \vec{\epsilon}) \subseteq \bigcup_{i \in \{1, \dots, n\}} U_1 \times \dots \times (U_i \setminus U_i + \epsilon) \times \dots \times U_n,$$

where this last set has measure bounded by  $nC^{n-1}\epsilon$ . With the previous inclusions, we get

$$\omega(\mathbb{R}^{2n+} \cap (U^2 \setminus V^2)) \leq 2n C^{n-1} \epsilon \omega(U).$$

Symmetrically, the Lebesgue measure of  $\mathbb{R}^{2n+} \cap (V^2 \setminus U^2)$  is bounded by  $2n (C')^{n-1} \epsilon \omega(V)$ . Finally, using that  $\omega(U) \leq C^n$ ,  $\omega(V) \leq (C')^n$  and (21) we obtain

$$\omega(\mathbb{R}^{2n+} \cap (U^2 \Delta V^2)) \leq 2n (C^{2n-1} + (C + 2\epsilon)^{2n-1}) \epsilon. \quad (23)$$

□

*Proof of Proposition 27.* Let

$$M = \bigoplus_{j \in \mathcal{J}} \mathbb{I}^{J_j} \quad \text{and} \quad N = \bigoplus_{k \in \mathcal{K}} \mathbb{I}^{K_k}$$

be the interval decompositions of  $M$  and  $N$ . Let  $\phi : \mathcal{I} \rightarrow \mathcal{K}$  be an injection of a subset  $\mathcal{I} \subset \mathcal{J}$  into  $\mathcal{K}$ . Given the additivity of rank invariant with respect to decompositions, we have

$$\begin{aligned} \|\beta^M - \beta^N\|_p &= \left\| \sum_{\phi(i)=k} \beta^{J_i} - \beta^{K_k} + \sum_{j \in \mathcal{J} \setminus \mathcal{I}} \beta^{J_j} - \sum_{k \in \mathcal{K} \setminus \phi(\mathcal{I})} \beta^{K_k} \right\|_p \\ &\leq \sum_{\phi(i)=k} \|\beta^{J_i} - \beta^{K_k}\|_p + \sum_{j \in \mathcal{J} \setminus \mathcal{I}} \|\beta^{J_j}\|_p + \sum_{k \in \mathcal{K} \setminus \phi(\mathcal{I})} \|\beta^{K_k}\|_p \\ &\leq c_{M,n}^{1/p} \left[ \sum_{\phi(i)=k} d_I(\mathbb{I}^{J_i}, \mathbb{I}^{K_k})^{1/p} + \sum_{j \in \mathcal{J} \setminus \mathcal{I}} d_I(\mathbb{I}^{J_j}, 0)^{1/p} + \sum_{k \in \mathcal{K} \setminus \phi(\mathcal{I})} d_I(0, \mathbb{I}^{K_k})^{1/p} \right]. \end{aligned} \quad (24)$$

For  $p = 1$ , taking the infimum over all the possible matchings in (24) we directly get

$$\|\beta^M - \beta^N\|_1 \leq c_{M,n} \cdot d_{W_1}(M, N).$$

For  $p = 2$ , we apply the Cauchy–Schwarz inequality twice to (24) and take the infimum over all matchings to find

$$\|\beta^M - \beta^N\|_2 \leq (3c_{M,n})^{1/2} \max\{|\mathcal{I}|^{1/2}, |\mathcal{J} \setminus \mathcal{I}|^{1/2}, |\mathcal{K} \setminus \phi(\mathcal{I})|^{1/2}\} \cdot d_{W_1}(M, N)^{1/2}$$

concluding the proof.  $\square$

Notice that for the  $L_1$  distance, the constant actually only depends on the persistence module  $M$ , as in the case of single-parameter persistence. This does not extend to the  $L_2$  distance.

**Stability under the Function-Interleaving Distance.** We now turn to studying a pseudometric inspired by the interleaving distance, but applied to rank invariants, and study its stability properties under our proposed pseudometric. Again, we are motivated by the ease of computation of metrics on functions, which leads us to compare the interleaving function with the infinity norm of an alternative functional summary of multiparameter persistence, the *multiparameter persistence landscape*.

The commutative diagram (22) in the proof of Lemma 28 gives us an inequality between the rank invariants of a pair of  $\epsilon$ -interleaved multiparameter persistence modules  $M, N \in \text{Vec}^{(\mathbb{R}^n, \preceq)}$ . The symmetry of  $M$  and  $N$  in this argument motivates the following definition.

**Definition 29** (Function-interleaving distance). Let  $f, g : \Omega \times \Omega \rightarrow \mathbb{R}$  be two real-valued functions, with  $\Omega \subset \mathbb{R}^n$ . We define the *function-interleaving distance* between  $f$  and  $g$  by

$$d_{\text{FI}}(f, g) = \inf\{\epsilon \geq 0 : f(x, y) \geq g(x - \vec{c}, y + \vec{c}) \text{ and } g(x, y) \geq f(x - \vec{c}, y + \vec{c}), \forall (x, y) \in \Omega \times \Omega\}$$

where  $\epsilon = \|\vec{c}\|_\infty$  for  $\vec{c} \in \mathbb{R}^n$ , and  $d_{\text{FI}}(f, g) = \infty$  if such  $\epsilon \geq 0$  does not exist.

**Lemma 30.** *The function-interleaving distance is an extended pseudometric in the space of rank invariants  $\mathcal{I}_n$ .*

*Proof.* From Definition 29, we have  $d_{\text{FI}}(\beta^M, \beta^M) = 0$  and  $d_{\text{FI}}(\beta^M, \beta^N) = d_{\text{FI}}(\beta^N, \beta^M)$  for every  $M, N \in \text{Vec}^{(\mathbb{R}^n, \preceq)}$ . To check that the triangle inequality is satisfied, let us consider  $M_1, M_2, M_3 \in \text{Vec}^{(\mathbb{R}^n, \preceq)}$  and  $\epsilon_1 \geq 0, \epsilon_2 \geq 0$  such that

$$\beta^{M_1}(x, y) \geq \beta^{M_2}(x - \vec{\epsilon}_1, y + \vec{\epsilon}_1), \quad \beta^{M_2}(x, y) \geq \beta^{M_1}(x - \vec{\epsilon}_1, y + \vec{\epsilon}_1); \quad (25)$$

$$\beta^{M_2}(x, y) \geq \beta^{M_3}(x - \vec{\epsilon}_2, y + \vec{\epsilon}_2), \quad \beta^{M_3}(x, y) \geq \beta^{M_2}(x - \vec{\epsilon}_2, y + \vec{\epsilon}_2) \quad (26)$$

for all  $(x, y) \in \mathbb{R}^{2n+}$ . Combining (25) and (26), we get

$$\begin{aligned} \beta^{M_1}(x, y) &\geq \beta^{M_2}(x - \vec{\epsilon}_1, y + \vec{\epsilon}_1) \geq \beta^{M_3}(x - (\vec{\epsilon}_1 + \vec{\epsilon}_2), y + (\vec{\epsilon}_1 + \vec{\epsilon}_2)); \\ \beta^{M_3}(x, y) &\geq \beta^{M_2}(x - \vec{\epsilon}_2, y + \vec{\epsilon}_2) \geq \beta^{M_1}(x - (\vec{\epsilon}_1 + \vec{\epsilon}_2), y + (\vec{\epsilon}_1 + \vec{\epsilon}_2)), \end{aligned} \quad (27)$$

implying that  $d_{\text{FI}}(\beta^{M_1}, \beta^{M_3}) \leq \vec{\epsilon}_1 + \vec{\epsilon}_2$ . Taking the infimum on the right side of (27), we conclude

$$d_{\text{FI}}(\beta^{M_1}, \beta^{M_3}) \leq d_{\text{FI}}(\beta^{M_1}, \beta^{M_2}) + d_{\text{FI}}(\beta^{M_2}, \beta^{M_3}).$$

$\square$

The function-interleaving distance fails to be a metric, even in the case of single-parameter persistence; a straightforward counterexample is the following, which also applies for the interleaving distance (see Example 2.3 from Lesnick, 2015): Let  $M \in \text{Vec}^{(\mathbb{R}, \leq)}$  be the persistence module such that  $M_0 = \mathbb{F}$  and  $M_t = 0$  for

$t \neq 0$ , and let  $N \in \text{Vec}^{(\mathbb{R}, \leq)}$  be the trivial persistence module  $N_s = 0$  for all  $s \in \mathbb{R}$ . These modules are not isomorphic, however, for every  $\epsilon \geq 0$ ,

$$\beta^M(x, y) \geq \beta^N(x - \vec{\epsilon}, y + \vec{\epsilon}) \text{ and } \beta^N(x, y) \geq \beta^M(x - \vec{\epsilon}, y + \vec{\epsilon}),$$

for all  $(x, y) \in \mathbb{R}^{2n+}$  so that  $d_{\text{FI}}(\beta^M, \beta^N) = 0$ .

Notice also that the function-interleaving distance on rank invariants from persistence modules  $M, N \in \text{Vec}^{(\mathbb{R}^n, \preceq)}$  with no essential cycles is always finite. Take  $\epsilon > 0$  to be the distance to the diagonal from the farthest point to it, which is finite. This value satisfies the conditions

$$\beta^M(x, y) \geq \beta^N(x - \vec{\epsilon}, y + \vec{\epsilon}) \text{ and } \beta^N(x, y) \geq \beta^M(x - \vec{\epsilon}, y + \vec{\epsilon}),$$

for all  $(x, y) \in \mathbb{R}^{2n+}$  which, from Definition 29, allows us to conclude that  $d_{\text{FI}}(f, g) \leq \epsilon < \infty$ .

An argument similar to the one involving the commutative diagram (22) in the proof of Lemma 28 appeared in the introduction of multiparameter persistence landscapes by Vipond (2020). Persistence landscapes were first defined by Bubenik (2015) in the framework of single-parameter persistence as a vectorization of persistence diagrams to incorporate persistence information in existing statistical and machine learning methodology. They are a modified version of rank functions satisfying a strong stability property on their infinite norm (see (28) for the definition of this distance), with respect to the interleaving distance between the persistence modules (Theorem 12, Bubenik (2015)). Their extension to the multiparameter setting is naturally obtained from their relation to rank invariants.

**Definition 31** (Multiparameter persistence landscapes, Vipond (2020)). Let  $M \in \text{Vec}^{(\mathbb{R}^n, \preceq)}$  be multiparameter persistence module and  $\beta^M$  its associated rank invariant. The *multiparameter persistence landscape* is the function defined by

$$\begin{aligned} \lambda : \mathbb{Z}_{\geq 0} \times \mathbb{R}^n &\rightarrow \mathbb{R} \\ (k, x) &\mapsto \sup\{h > 0 : \beta^M(x - h \vec{1}, x + h \vec{1}) \geq k\}, \end{aligned}$$

where  $\vec{1} := (1, \dots, 1)$ . The space of persistence landscapes for  $n$ -dimensional persistence modules is denoted by  $\mathcal{L}_n$ .

Although rank invariants and multiparameter persistence landscapes are both functional summaries of multiparameter persistent homology, notice that there is nevertheless an important difference in the nature of how they capture persistence information: rank functions, by their Möbius inversion construction, identically capture persistent homology, while Vipond (2020) proves an injectivity result that multiparameter landscapes capture most, but not all, of the information associated with their persistence modules (Vipond, 2020, Proposition 36).

Notice that, as functions with domain  $\mathbb{Z}_{\geq 0} \times \mathbb{R}^n$ , we can use  $L^p$  distances,  $1 \leq p \leq \infty$ , to compare the persistence landscapes of  $M, N \in \text{Vec}^{(\mathbb{R}^n, \preceq)}$ :

$$d_\lambda^p(M, N) := \|\lambda(M) - \lambda(N)\|_p. \quad (28)$$

The stability result originally proved by Bubenik (2015) in single-parameter persistence also extends naturally to the multiparameter framework.

**Theorem 32** (Theorem 30, Vipond (2020)). *For  $M, N \in \text{Vec}^{(\mathbb{R}^n, \preceq)}$  multiparameter persistence modules, we have*

$$d_\lambda^\infty(M, N) \leq d_I(M, N).$$

We now prove the following theorem which demonstrates that the function-interleaving distance is better able to discriminate shapes than the  $d_\lambda^\infty$  distance on persistence landscapes, while also being stable with respect to the interleaving distance.

**Theorem 33.** Let  $M, N : (\mathbb{R}^n, \preceq) \rightarrow \text{Vec}$  be two persistence modules;  $\beta^M, \beta^N$  their associated rank invariants; and  $\lambda^M, \lambda^N$  their persistence landscapes. We have

$$d_\lambda^\infty(M, N) \leq d_{\text{FI}}(\beta^M, \beta^N) \leq d_I(M, N). \quad (29)$$

*Proof.* The second inequality in (29) is a straightforward consequence of the definition of the function-interleaving distance (see Definition 29), so we turn to the proof of the first inequality, comparing the  $d^\infty$  distance of persistence landscapes and the function-interleaving distance.

Let  $M, N$  be two p.f.d.  $\mathbb{R}^n$ -persistence modules;  $\beta^M, \beta^N$  their associated rank functions; and  $\lambda^M, \lambda^N$  their associated persistence landscapes. Call  $r := d_{\text{FI}}(\beta^M, \beta^N)$  and fix  $k \in \mathbb{N}_{>0}$  and  $x \in \mathbb{R}^n$ .

If  $\lambda^N(k, x) - r \leq 0$ , we directly obtain that  $\lambda^M(k, x) \geq \lambda^N(k, x) - r$ , so we turn to the case where  $\lambda^N(k, x) - r > 0$ . For every  $0 < h < \lambda^N(k, x) - r$ , take  $r' > r$  such that  $h + r' < \lambda^N(k, x)$ , which gives

$$\beta^M(x - h \vec{1}, x + h \vec{1}) \geq \beta^N(x - (h + r') \vec{1}, x + (h + r') \vec{1}) \geq k,$$

meaning that  $\lambda^M(k, x) \geq h$ . Seeing that this holds for any  $0 < h < \lambda^N(k, x) - r$ , we get  $\lambda^M(k, x) \geq \lambda^N(k, x) - r$ . Symmetrically, interchanging the modules  $N$  and  $M$  we can obtain  $\lambda^N(k, x) \geq \lambda^M(k, x) - r$ , proving that  $d_\lambda^\infty(M, N) \leq r$ , as desired.  $\square$

An interesting particular case of Theorem 33 holds in the case of single-parameter persistence. If  $M = \bigoplus_{j \in J} \mathbb{I}[b_j, d_j]$  is a p.f.d.  $\mathbb{R}$ -module and  $r > 0$ , we denote

$$M_r := \bigoplus_{j \in J} \mathbb{I}[b_j - r, d_j + r].$$

With this notation, we have that  $\lambda^M + r = \lambda^{M_r}$ , and for all  $x \leq y$ ,  $\beta^M(x, y) = \beta^{M_r}(x - r, y + r)$ .

**Proposition 34.** In the case of single-parameter persistence, the map  $(\mathcal{I}_1, d_{\text{FI}}) \rightarrow (\mathcal{L}_1, d_\lambda^\infty)$  is an isometry.

*Proof.* From Theorem 33, it suffices to prove that  $d_{\text{FI}}(\beta^M, \beta^N) \leq d_\lambda^\infty(M, N)$  for all p.f.d. modules  $M$  and  $N$ . Let  $\beta^M, \beta^N$  be their associated rank functions and  $\lambda^M, \lambda^N$  their associated persistence landscapes. Take  $r = d_\lambda^\infty(M, N)$ . Then we have  $\lambda^M + r \geq \lambda^N$ , i.e.,  $\lambda^{M_r} \geq \lambda^N$ . Therefore,  $\beta^{M_r} \geq \beta^N$ , which means that

$$\beta^M(x, y) = \beta^{M_r}(x - r, y + r) \geq \beta^N(x - r, y + r).$$

Symmetrically, we have  $\beta^{N_r} \geq \beta^M$ , and we conclude that  $d_{\text{FI}}(\beta^M, \beta^N) \leq r$ .  $\square$

## 5 Discussion

In this paper, we have demonstrated the applicability of rank functions and rank invariants in inferential ML tasks on both real and simulated data with significantly improved results over other techniques that do not entail persistence geared to the same inference tasks. We then validated these results by providing *computable* stability guarantees, by focusing on computationally efficient and feasible metrics for both single and multiparameter persistent homology. In studying rank invariants in the multiparameter setting, we introduced a function-interleaving distance which takes inspiration from the universal interleaving distance for persistent homology as well as the functional nature of our study. We furthermore explored the relationship in terms of stability between rank invariants and multiparameter persistence landscapes as the main functional invariants in the multiparameter persistence literature.

From the perspective of applications, the driving limitation, especially in multiparameter persistence, is computational expense. While computational efficiency was not the focus of our work, the practical applications we have shown on both real and simulated data as well as the theoretical justifications we established

provide a solid basis and motivation towards an improved computational efficiency for multiparameter persistence, and especially for rank functions. This would then greatly extend the reach of applicability of multiparameter persistence and open the door for a more thorough understanding of the statistical potential of multiparameter persistent homology.

Regarding our theoretical stability contributions, a natural extension of this work would be to explore the possibility of improving the bounds and achieving tightness for single-parameter rank function stability. The definition of the function-interleaving distance also opens the door to a rigorous study of its properties and relations to other computable and more theoretical metrics for rank invariants.

## Software & Data Availability

All code and data to reproduce results in this paper are available from [https://github.com/Qiquan-Wang/rank\\_stability](https://github.com/Qiquan-Wang/rank_stability). The heart rate variability data were collected and studied by Gąsecki et al. (2021) and Narkiewicz et al. (2021). The lung imaging LIDC data were obtained from TCIA Armato III et al. (2011).

## Acknowledgements

We wish to thank Yueqi Cao, Lorin Crawford, Herbert Edelsbrunner, Claudia Landi, Amit Patel, and Nicole Solomon for helpful discussions. Q.W. is grateful to Matthew Williams for his support and guidance. G.H.P. and A.M. also wish to acknowledge the Max-Planck Institute for Mathematics in the Sciences in Leipzig, Germany for hosting their visit in February 2018, where this work began.

This work was supported by the Engineering and Physical Sciences Research Council [EP/S021590/1]. The EPSRC Centre for Doctoral Training in Geometry and Number Theory (The London School of Geometry and Number Theory), University College London. I.G.R. is funded by the UK EPSRC London School of Geometry and Number Theory and Imperial College London.

Q.W. is funded by a CRUK–Imperial College London Convergence Science PhD studentship at the UK EPSRC Centre for Doctoral Training in Modern Statistics and Machine Learning (2021 cohort, PIs Monod/Williams).

# Figures

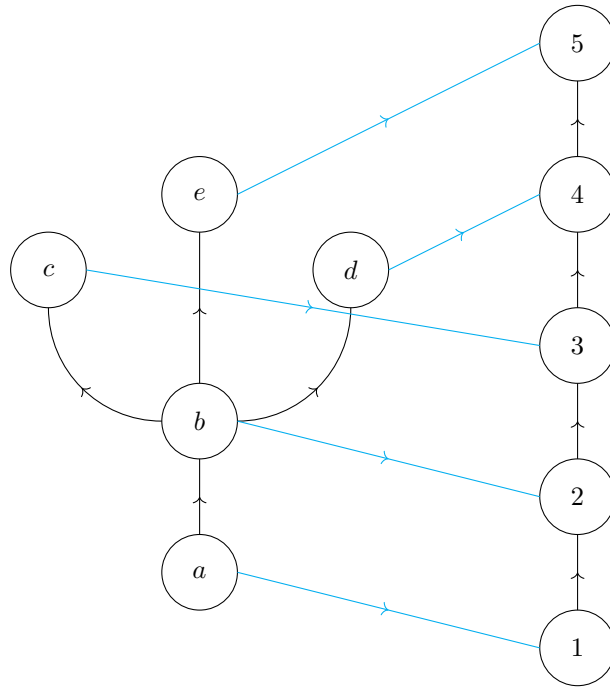


Figure 1: Example of a poset and its associated total/linear ordering.

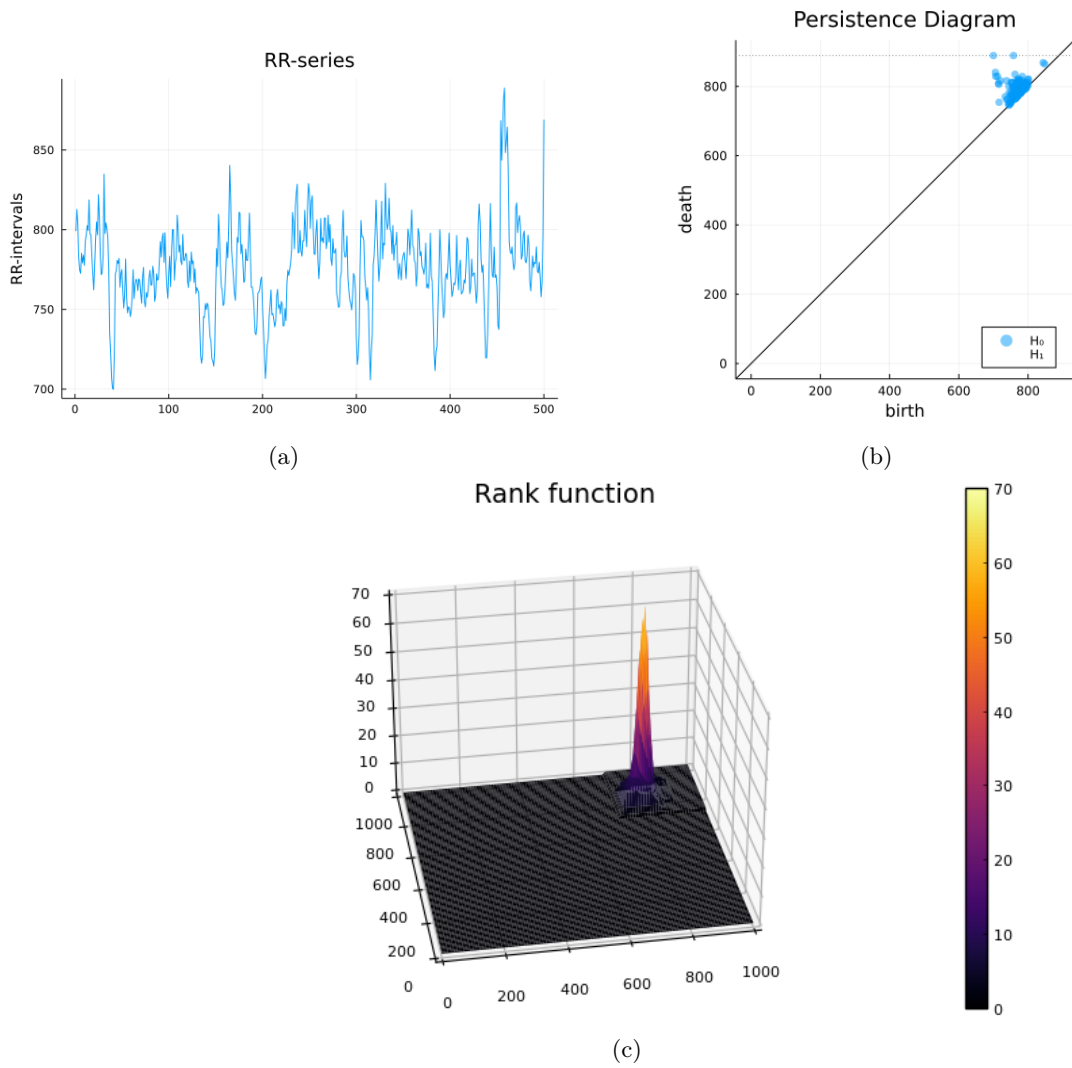
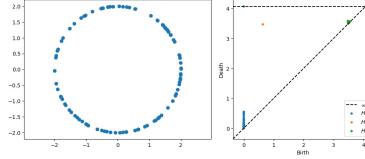
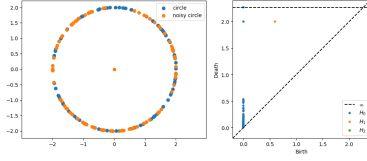


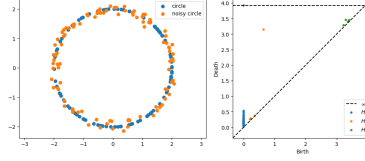
Figure 2: An example showing the RR series for a healthy individual (a), its respective persistence diagram (b) and rank function (c).



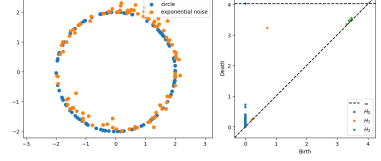
(a) Sample from circle with PD



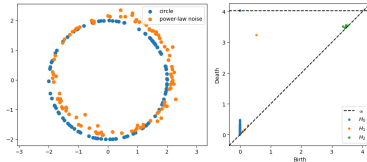
(b) Sample of Noise 1 with PD



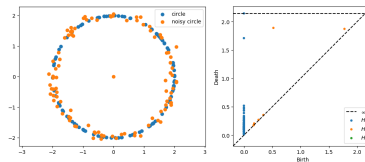
(c) Sample of Noise 2 with PD



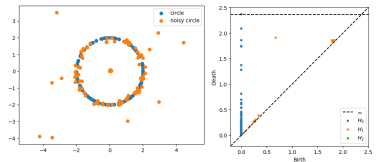
(d) Sample of Noise 3 with PD



(e) Sample of Noise 4 with PD



(f) Sample of Noise 5 with PD



(g) Sample of Noise 6 with PD

Figure 3: Figure 3(a) shows an example of 100 sampled points from the circle of radius two and its corresponding persistence diagram computed from Vietoris–Rips filtration on the points. Figures 3(b) to 3(g) show plots of noisy samples with their corresponding persistence diagrams, where the different types of noise are as outlined in Section 3.2.

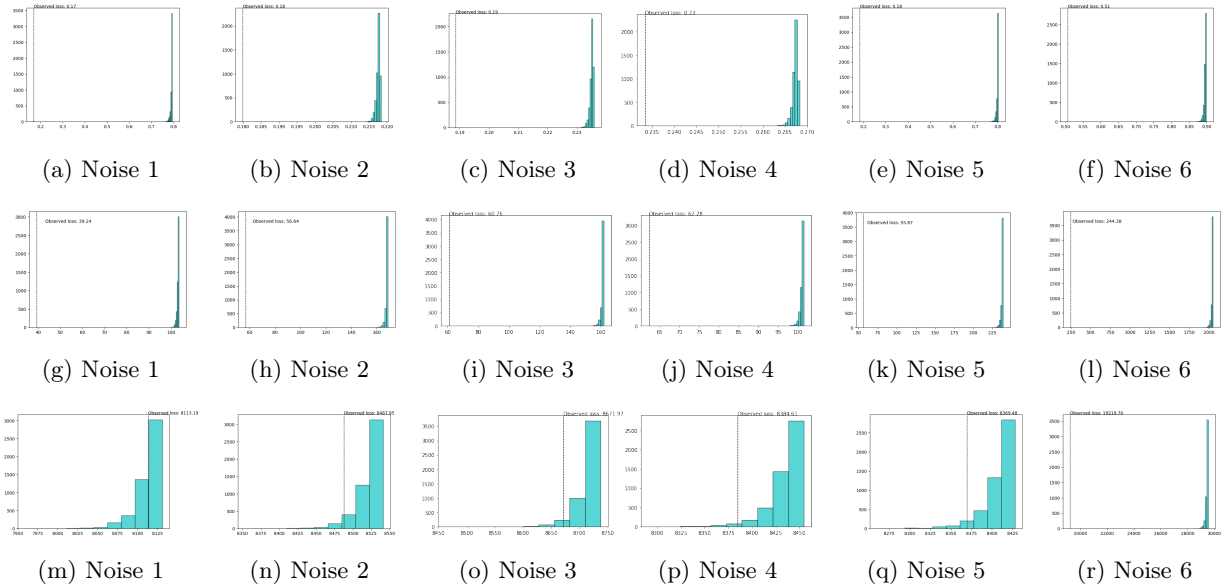
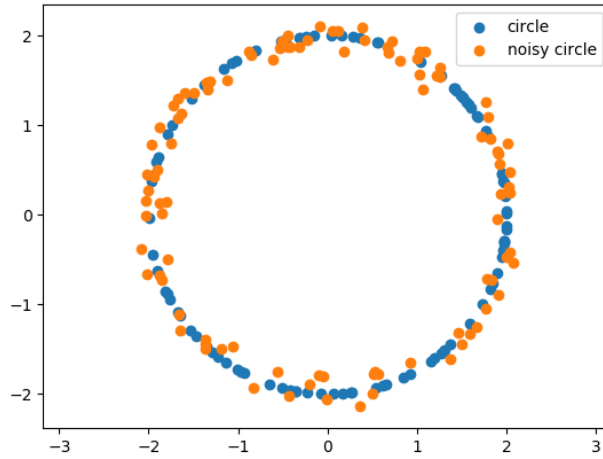
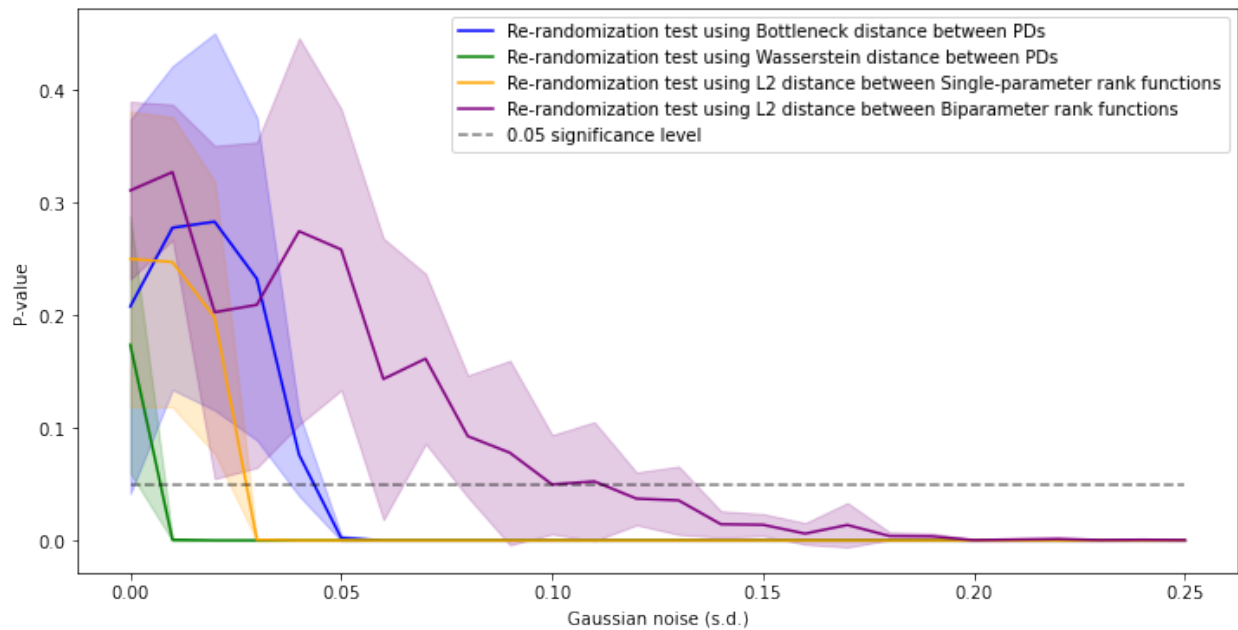


Figure 4: Figures 4(a) to 4(f) show the distributions of the test statistic (computed on  $(\mathcal{D}_2, d_B)$ ) under the null hypothesis from Monte Carlo simulations where the two collections of samples considered are those sample from the circle and those sampled from the circle with noise as specified in the caption and illustrated above. Similarly, Figures 4(g) to 4(l) show the distributions of the test statistic computed on  $(\mathcal{I}_1, L^2)$ . Lastly, Figures 4(m) to 4(r) show the distributions of the test statistic computed on  $(\mathcal{I}_2, L^2)$ .

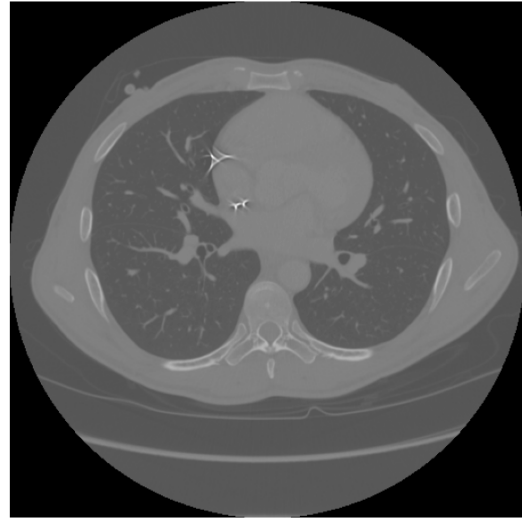
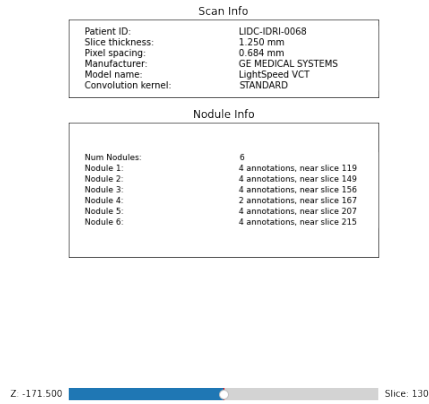


(a)

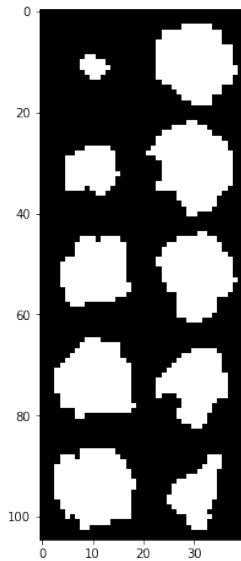


(b)

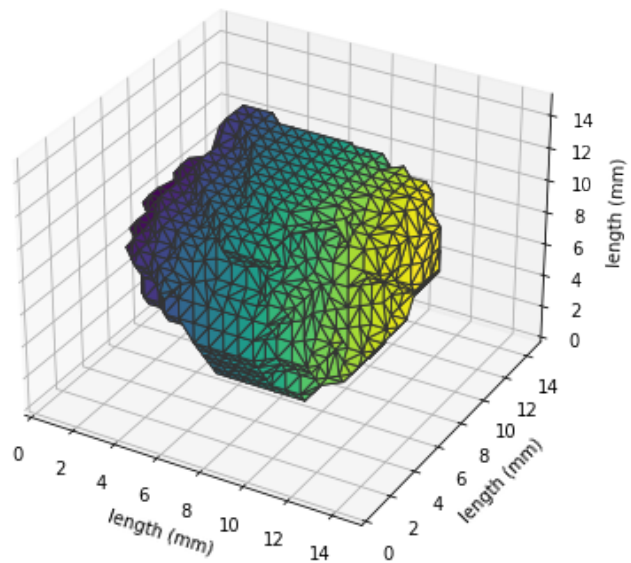
Figure 5: Figure (a) shows sampled points from the circle with added Gaussian noise with standard deviations of 0.1 overlaid on points simulated on the circle. Figure (b) shows trends of mean p-values for Re-randomization tests between samples from the circle and samples from the circle with added noise over increasing (standard deviation of) Gaussian noise plotted with  $\pm 1$  s.d.



(a)



(b)



(c)

Figure 6: An example showing the data extraction process. Annotated CT images (a) from the LIDC combined with masks (b) are converted into a 3D surface (c) from which we can sample a point cloud.

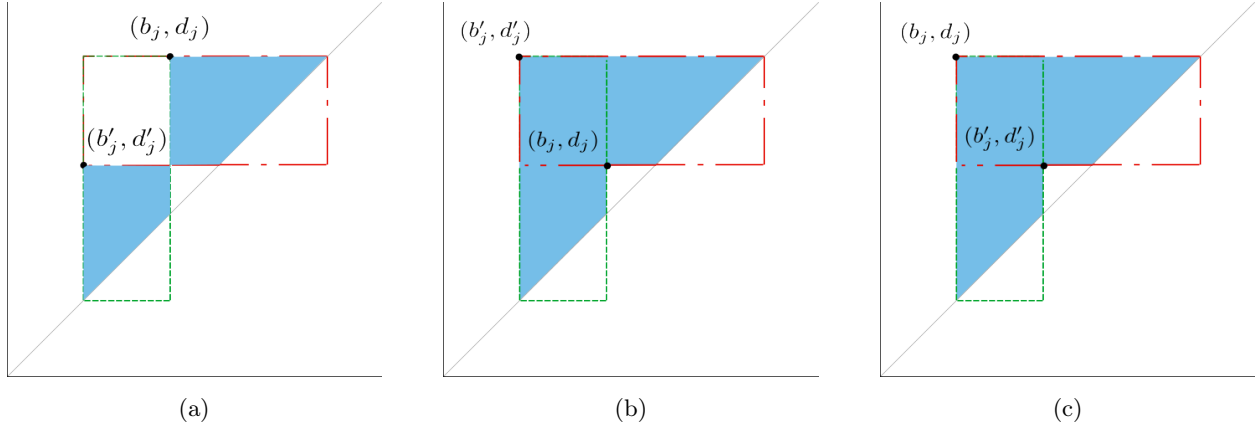


Figure 7: Example of domains  $D_j$  (shaded in blue) on which rank functions differ and the sketched rectangles (delineated by red dashed lines and green dotted lines) indicate the bound of  $\omega(D_j^c)$  when  $M = \mathbb{I}[b_j, d_j]$  and  $N = \mathbb{I}[b'_j, d'_j]$ .

## Tables

Table 1: Accuracy and AUC-ROCs of classifiers constructed on rank functions data and projected data with linear, GRBF, and polynomial kernels over ten iterations of five-fold cross validation.

Kernel	Discretized rank functions		Projected rank functions on			
			Principal component basis functions		Wavelet basis functions	
	Accuracy	AUC-ROC	Accuracy	AUC-ROC	Accuracy	AUC-ROC
Linear	39.5%	0.408	66.8%	0.681	39.7%	0.404
GRBF	75.8%	0.762	50.3%	0.502	75.0%	0.756
Polynomial (d=2)	82.6%	0.829	84.2%	0.842	84.0%	0.842
Polynomial (d=3)	81.6%	0.829	82.0%	0.829	80.3%	0.816
Polynomial (d=5)	76.0%	0.775	75.5%	0.774	76.6%	0.786

Table 2: Table of  $p$ -values from permutation testing between 100 samples generated from the circle and 100 samples generated from the circle with various types of noise/outliers ( $p$ -values are estimated from 5000 iterations of Monte Carlo simulation).

	Noise 1	Noise 2	Noise 3	Noise 4	Noise 5	Noise 6
Persistence Diagrams	0.0002	0.0002	0.0002	0.0002	0.0002	0.0002
1-parameter rank functions	0.0002	0.0002	0.0002	0.0002	0.0002	0.0002
Biparameter rank invariants	0.3659	0.0554	0.0368	0.0218	0.0478	0.0002

Table 3: Table of average percentage accuracy and AUC-ROC of classification between benign and malignant primary tumors in the LIDC dataset containing 29 benign tumour samples and 41 malignant tumor samples.

		$k$ -NN		$MBD$	
		Accuracy	AUC-ROC	Accuracy	AUC-ROC
Primary Benign vs Malignant	$h$ -Rips	61.4	59.9	68.8	69.1
	$x$ -Rips	64.4	64.2	67.9	68.2
	$y$ -Rips	61.2	60.4	70.0	71.0
	Degree-Rips	63.3	61.8	70.8	72.0

Table 4: Table of average percentage accuracy and AUC-ROC of classification between benign and malignant primary tumors in LIDC dataset with added contrast material containing 24 benign tumor samples and 17 malignant tumor samples.

		$k$ -NN		$MBD$	
		Accuracy	AUC-ROC	Accuracy	AUC-ROC
Primary Benign vs Malignant (with contrast)	$h$ -Rips	83.8	83.0	76.9	76.8
	$x$ -Rips	80.2	79.1	80.7	79.9
	$y$ -Rips	79.6	78.5	80.0	79.3
	Degree-Rips	80.0	79.1	72.5	72.7

## References

- Adams, H., T. Emerson, M. Kirby, R. Neville, C. Peterson, P. Shipman, S. Chepushtanova, E. Hanson, F. Motta, and L. Ziegelmeier (2017). Persistence images: A stable vector representation of persistent homology. *The Journal of Machine Learning Research* 18(1), 218–252.
- Adler, R. J., O. Bobrowski, M. S. Borman, E. Subag, and S. Weinberger (2010). *Persistent homology for random fields and complexes*, Volume Volume 6 of *Collections*, pp. 124–143. Beachwood, Ohio, USA: Institute of Mathematical Statistics.
- Adler, R. J., O. Bobrowski, and S. Weinberger (2014). Crackle: The homology of noise. *Discrete & Computational Geometry* 52, 680–704.
- Armato III, S. G., G. McLennan, L. Bidaut, M. F. McNitt-Gray, C. R. Meyer, A. P. Reeves, B. Zhao, D. R. Aberle, C. I. Henschke, E. A. Hoffman, E. A. Kazerooni, H. MacMahon, E. J. R. van Beek, D. Yankelevitz, A. M. Biancardi, P. H. Bland, M. S. Brown, R. M. Engelmann, G. E. Laderach, D. Max, R. C. Pais, D. P.-Y. Qing, R. Y. Roberts, A. R. Smith, A. Starkey, P. Batra, P. Caligiuri, A. Farooqi, G. W. Gladish, C. M. Jude, R. F. Munden, I. Petkovska, L. E. Quint, L. H. Schwartz, B. Sundaram, L. E. Dodd, C. Fenimore, D. Gur, N. Petrick, J. Freymann, J. Kirby, B. Hughes, A. Vande Castele, S. Gupte, M. Sallam, M. D. Heath, M. H. Kuhn, E. Dharaiya, R. Burns, D. S. Fryd, M. Salganicoff, V. Anand, U. Shreter, S. Vastagh, B. Y. Croft, and L. P. Clarke (2011). The lung image database consortium (lidc) and image database resource initiative (idri): A completed reference database of lung nodules on ct scans. *Medical Physics* 38(2), 915–931.
- Armato III, S. G., G. McLennan, L. Bidaut, M. F. McNitt-Gray, C. R. Meyer, A. P. Reeves, B. Zhao, D. R. Aberle, C. I. Henschke, E. A. Hoffman, E. A. Kazerooni, H. MacMahon, E. J. R. Van Beek, D. Yankelevitz, A. M. Biancardi, P. H. Bland, M. S. Brown, R. M. Engelmann, G. E. Laderach, D. Max, R. C. Pais, D. P. Y. Qing, R. Y. Roberts, A. R. Smith, A. Starkey, P. Batra, P. Caligiuri, A. Farooqi, G. W. Gladish, C. M. Jude, R. F. Munden, I. Petkovska, L. E. Quint, L. H. Schwartz, B. Sundaram, L. E. Dodd, C. Fenimore, D. Gur, N. Petrick, J. Freymann, J. Kirby, B. Hughes, A. V. Castele, S. Gupte, M. Sallam, M. D. Heath, M. H. Kuhn, E. Dharaiya, R. Burns, D. S. Fryd, M. Salganicoff, V. Anand, U. Shreter, S. Vastagh, B. Y. Croft, and L. P. Clarke (2015). Data from lidc-idri.
- Atienza, N., R. Gonzalez-Díaz, and M. Soriano-Trigueros (2020). On the stability of persistent entropy and new summary functions for topological data analysis. *Pattern Recognition* 107, 107509.
- Bauer, U. and M. Lesnick (2015, March). Induced matchings and the algebraic stability of persistence barcodes. *Journal of Computational Geometry* 6(2), 162–191. Number: 2.
- Biasotti, S., A. Cerri, P. Frosini, D. Giorgi, and C. Landi (2008). Multidimensional Size Functions for Shape Comparison. *Journal of Mathematical Imaging and Vision* 32(2), 161–179.
- Biasotti, S., L. De Floriani, B. Falcidieno, P. Frosini, D. Giorgi, C. Landi, L. Papaleo, and M. Spagnuolo (2008). Describing shapes by geometrical-topological properties of real functions. *ACM Comput. Surv.* 40(4), 12:1–12:87.
- Bjerkevik, B. H. (2021, July). On the Stability of Interval Decomposable Persistence Modules. *Discrete & Computational Geometry* 66(1), 92–121.
- Bjerkevik, H. B., M. B. Botnan, and M. Kerber (2020, October). Computing the Interleaving Distance is NP-Hard. *Foundations of Computational Mathematics* 20(5), 1237–1271.

- Bjerkevik, H. B. and M. Lesnick (2021, November).  $\ell^p$ -Distances on Multiparameter Persistence Modules. arXiv:2106.13589 [cs, math].
- Blumberg, A. J., I. Gal, M. A. Mandell, and M. Pancia (2014, Aug). Robust Statistics, Hypothesis Testing, and Confidence Intervals for Persistent Homology on Metric Measure Spaces. *Foundations of Computational Mathematics* 14(4), 745–789.
- Bobrowski, O. and M. Kahle (2018, 1). Topology of random geometric complexes: a survey. *Journal of Applied and Computational Topology*, 1–34.
- Boser, B. E., I. M. Guyon, and V. N. Vapnik (1992). A training algorithm for optimal margin classifiers. In *Proceedings of the Fifth Annual Workshop on Computational Learning Theory, COLT '92*, New York, NY, USA, pp. 144–152. Association for Computing Machinery.
- Botnan, M. and W. Crawley-Boevey (2020, August). Decomposition of persistence modules. *Proceedings of the American Mathematical Society* 148(11), 4581–4596.
- Botnan, M. B., S. Oppermann, and S. Oudot (2022). Signed Barcodes for Multi-Parameter Persistence via Rank Decompositions. In X. Goaoc and M. Kerber (Eds.), *38th International Symposium on Computational Geometry (SoCG 2022)*, Volume 224 of *Leibniz International Proceedings in Informatics (LIPIcs)*, Dagstuhl, Germany, pp. 19:1–19:18. Schloss Dagstuhl – Leibniz-Zentrum für Informatik.
- Bramer, D. and G.-W. Wei (2020, January). Atom-specific persistent homology and its application to protein flexibility analysis. *Computational and Mathematical Biophysics* 8(1), 1–35. Publisher: De Gruyter Open Access.
- Bubenik, P. (2015). Statistical topological data analysis using persistence landscapes. *The Journal of Machine Learning Research* 16(1), 77–102.
- Bubenik, P., V. de Silva, and J. Scott (2015, December). Metrics for generalized persistence modules. *Foundations of Computational Mathematics* 15(6), 1501–1531. arXiv:1312.3829 [cs, math].
- Bubenik, P., J. Scott, and D. Stanley (2023, June). Exact weights, path metrics, and algebraic Wasserstein distances. *Journal of Applied and Computational Topology* 7(2), 185–219.
- Bubenik, P. and J. A. Scott (2014, April). Categorification of persistent homology. *Discrete & Computational Geometry* 51(3), 600–627.
- Burley, S. K., C. Bhikadiya, C. Bi, S. Bittrich, L. Chen, G. V. Crichlow, C. H. Christie, K. Dalenberg, L. Di Costanzo, J. M. Duarte, S. Dutta, Z. Feng, S. Ganesan, D. S. Goodsell, S. Ghosh, R. K. Green, V. Guranović, D. Guzenko, B. P. Hudson, C. Lawson, Y. Liang, R. Lowe, H. Namkoong, E. Peisach, I. Persikova, C. Randle, A. Rose, Y. Rose, A. Sali, J. Segura, M. Sekharan, C. Shao, Y.-P. Tao, M. Voigt, J. Westbrook, J. Y. Young, C. Zardecki, and M. Zhuravleva (2021, January). RCSB Protein Data Bank: powerful new tools for exploring 3D structures of biological macromolecules for basic and applied research and education in fundamental biology, biomedicine, biotechnology, bioengineering and energy sciences. *Nucleic Acids Research* 49(D1), D437–D451.
- Cagliari, F., M. Ferri, and P. Pozzi (2001). Size Functions from a Categorical Viewpoint. *Acta Applicandae Mathematica* 67(3), 225–235.
- Cang, Z., L. Mu, and G.-W. Wei (2018, January). Representability of algebraic topology for biomolecules in machine learning based scoring and virtual screening. *PLOS Computational Biology* 14(1), e1005929. Publisher: Public Library of Science.

- Cang, Z. and G.-W. Wei (2017, November). Analysis and prediction of protein folding energy changes upon mutation by element specific persistent homology. *Bioinformatics* 33(22), 3549–3557.
- Cao, Y., P. Leung, and A. Monod (2022).  $k$ -means clustering for persistent homology. *arXiv preprint arXiv:2210.10003*.
- Cao, Y. and A. Monod (2022a, May). Approximating Persistent Homology for Large Datasets. arXiv:2204.09155 [cs, math, stat].
- Cao, Y. and A. Monod (2022b). A Geometric Condition for Uniqueness of Fréchet Means of Persistence Diagrams. *arXiv preprint arXiv:2207.03943*.
- Carlsson, G. and V. de Silva (2010). Zigzag persistence. *Foundations of computational mathematics* 10(4), 367–405.
- Carlsson, G. and A. Zomorodian (2007, 06). The theory of multidimensional persistence. *Discrete and Computational Geometry* 42, 71–93.
- Carlsson, G. and A. Zomorodian (2009, July). The Theory of Multidimensional Persistence. *Discrete & Computational Geometry* 42(1), 71–93.
- Cerri, A., B. D. Fabio, M. Ferri, P. Frosini, and C. Landi (2013). Betti numbers in multidimensional persistent homology are stable functions. *Mathematical Methods in the Applied Sciences* 36(12), 1543–1557.
- Chazal, F., D. Cohen-Steiner, M. Glisse, L. J. Guibas, and S. Y. Oudot (2009, June). Proximity of persistence modules and their diagrams. In *Proceedings of the twenty-fifth annual symposium on Computational geometry*, SCG '09, New York, NY, USA, pp. 237–246. Association for Computing Machinery.
- Chazal, F., V. De Silva, M. Glisse, and S. Oudot (2016). *The Structure and Stability of Persistence Modules*. SpringerBriefs in Mathematics. Cham: Springer International Publishing.
- Chazal, F., B. T. Fasy, F. Lecci, A. Rinaldo, and L. Wasserman (2014). Stochastic convergence of persistence landscapes and silhouettes. In *Proceedings of the thirtieth annual symposium on Computational geometry*, pp. 474. ACM.
- Chazal, F., M. Glisse, C. Labruère, and B. Michel (2015). Convergence rates for persistence diagram estimation in topological data analysis. *Journal of Machine Learning Research* 16, 3603–3635.
- Cohen-Steiner, D., H. Edelsbrunner, and J. Harer (2007, January). Stability of Persistence Diagrams. *Discrete & Computational Geometry* 37(1), 103–120.
- Cover, T. and P. Hart (1967). Nearest neighbor pattern classification. *IEEE Transactions on Information Theory* 13(1), 21–27.
- Cox, D. D. and J. S. Lee (2008). Pointwise testing with functional data using the westfall–young randomization method. *Biometrika* 95, 621–634.
- Crawford, L., A. Monod, A. X. Chen, S. Mukherjee, and R. Rabadán (2020). Predicting clinical outcomes in glioblastoma: An application of topological and functional data analysis. *Journal of the American Statistical Association* 115(531), 1139–1150.
- Crawley-Boevey, W. (2015, June). Decomposition of pointwise finite-dimensional persistence modules. *Journal of Algebra and Its Applications* 14(05), 1550066. Publisher: World Scientific Publishing Co.

- d'Amico, M., P. Frosini, and C. Landi (2003). Optimal matching between reduced size functions. *DISMI, Universit'a di Modena e Reggio Emilia* 35.
- d'Amico, M., P. Frosini, and C. Landi (2006). Using matching distance in size theory: A survey. *International Journal of Imaging Systems and Technology* 16(5), 154–161.
- d'Amico, M., P. Frosini, and C. Landi (2010). Natural Pseudo-Distances and Optimal Matching between Reduced Size Functions. *Acta Applicandae Mathematicae* 109(2), 527–554.
- Dauxois, J., A. Pousse, and Y. Romain (1982). Asymptotic theory for the principal component analysis of a vector random function: some applications to statistical inference. *Journal of multivariate analysis* 12(1), 136–154.
- Di Fabio, B., C. Landi, and F. Medri (2009). Recognition of Occluded Shapes Using Size Functions. In P. Foggia, C. Sansone, and M. Vento (Eds.), *Image Analysis and Processing – ICIAP 2009*, Berlin, Heidelberg, pp. 642–651. Springer Berlin Heidelberg.
- Edelsbrunner, Letscher, and Zomorodian (2002, November). Topological Persistence and Simplification. *Discrete & Computational Geometry* 28(4), 511–533.
- Fasy, B. T., F. Lecci, A. Rinaldo, L. Wasserman, S. Balakrishnan, and A. Singh (2014, 12). Confidence sets for persistence diagrams. *Ann. Statist.* 42(6), 2301–2339.
- Frosini, P. (1992). Measuring shapes by size functions. In *Intelligent Robots and Computer Vision X: Algorithms and Techniques*, Volume 1607, pp. 122–134. International Society for Optics and Photonics.
- Frosini, P. and C. Landi (1999). Size theory as a topological tool for computer vision. *Pattern Recognition and Image Analysis* 9(4), 596–603.
- Frosini, P. and C. Landi (2001, August). Size Functions and Formal Series. *Applicable Algebra in Engineering, Communication and Computing* 12(4), 327–349.
- Gamble, J. and G. Heo (2010, October). Exploring uses of persistent homology for statistical analysis of landmark-based shape data. *Journal of Multivariate Analysis* 101(9), 2184–2199.
- Gąsecki, D., B. Graff, A. Rojek, K. Narkiewicz, G. Graff, and P. Pilarczyk (2021). The database of normal rr-intervals of length up to 512 of 41 patients at rest hospitalized due to the episode of acute ischemic stroke.
- Gidea, M. (2017). Topological Data Analysis of Critical Transitions in Financial Networks. In E. Shmueli, B. Barzel, and R. Puzis (Eds.), *3rd International Winter School and Conference on Network Science*, Springer Proceedings in Complexity, Cham, pp. 47–59. Springer International Publishing.
- Graff, G., B. Graff, P. Pilarczyk, G. Jabłoński, D. Gąsecki, and K. Narkiewicz (2021). Persistent homology as a new method of the assessment of heart rate variability. *Plos one* 16(7), e0253851.
- Häberle, K., B. Bravi, and A. Monod (2023). Wavelet-Based Density Estimation for Persistent Homology. *arXiv preprint arXiv:2305.08999*.
- Hamilton, W., J. E. Borgert, T. Hamelryck, and J. S. Marron (2022). Persistent Topology of Protein Space. In E. Gasparovic, V. Robins, and K. Turner (Eds.), *Research in Computational Topology 2*, Association for Women in Mathematics Series, pp. 223–244. Cham: Springer International Publishing.

- Harrington, H. A., N. Otter, H. Schenck, and U. Tillmann (2019, January). Stratifying Multiparameter Persistent Homology. *SIAM Journal on Applied Algebra and Geometry* 3(3), 439–471. Publisher: Society for Industrial and Applied Mathematics.
- Hofer, C., R. Kwitt, M. Niethammer, and A. Uhl (2017). Deep learning with topological signatures. In I. Guyon, U. V. Luxburg, S. Bengio, H. Wallach, R. Fergus, S. Vishwanathan, and R. Garnett (Eds.), *Advances in Neural Information Processing Systems 30*, pp. 1634–1644. Curran Associates, Inc.
- Kerber, M., M. Lesnick, and S. Oudot (2019). Exact Computation of the Matching Distance on 2-Parameter Persistence Modules. pp. 15 pages. Artwork Size: 15 pages Medium: application/pdf Publisher: Schloss Dagstuhl - Leibniz-Zentrum fuer Informatik GmbH, Wadern/Saarbruecken, Germany Version Number: 1.0.
- Kerber, M. and A. Rolle (2021, January). Fast Minimal Presentations of Bi-graded Persistence Modules. In *2021 Proceedings of the Symposium on Algorithm Engineering and Experiments (ALENEX)*, Proceedings, pp. 207–220. Society for Industrial and Applied Mathematics.
- Kim, W. and F. Mémoli (2021, December). Generalized persistence diagrams for persistence modules over posets. *Journal of Applied and Computational Topology* 5(4), 533–581.
- Landi, C. (2018). *The Rank Invariant Stability via Interleavings*, pp. 1–10. Cham: Springer International Publishing.
- Landi, C. and P. Frosini (1997). New pseudodistances for the size function space. In *Vision Geometry VI*, Volume 3168, pp. 52–61. International Society for Optics and Photonics.
- Landi, C. and P. Frosini (2002). Size functions as complete invariants for image recognition. In *Vision Geometry XI*, Volume 4794, pp. 101–110. International Society for Optics and Photonics.
- Lees, T., F. Shad-Kaneez, A. M. Simpson, N. T. Nassif, Y. Lin, and S. Lal (2018). Heart rate variability as a biomarker for predicting stroke, post-stroke complications and functionality. *Biomarker Insights* 13.
- Lesnick, M. (2015, June). The Theory of the Interleaving Distance on Multidimensional Persistence Modules. *Foundations of Computational Mathematics* 15(3), 613–650.
- Lesnick, M. and M. Wright (2015, December). Interactive Visualization of 2-D Persistence Modules. arXiv:1512.00180 [cs, math] version: 1.
- Lesnick, M. and M. Wright (2022, June). Computing Minimal Presentations and Bigraded Betti Numbers of 2-Parameter Persistent Homology. *SIAM Journal on Applied Algebra and Geometry* 6(2), 267–298. Publisher: Society for Industrial and Applied Mathematics.
- López-Pintado, S. and J. Romo (2009). On the concept of depth for functional data. *Journal of the American Statistical Association* 104(486), 718–734.
- Marchese, A., V. Maroulas, and J. Mike (2017). K-means clustering on the space of persistence diagrams. In *Wavelets and Sparsity XVII*, Volume 10394, pp. 218–227. SPIE.
- Mileyko, Y., S. Mukherjee, and J. Harer (2011). Probability measures on the space of persistence diagrams. *Inverse Problems* 27(12), 124007.
- Miller, E. (2020, August). Data structures for real multiparameter persistence modules. arXiv:1709.08155 [math].

- Narkiewicz, K., B. Graff, G. Graff, and P. Pilarczyk (2021). The database of normal rr-intervals of length up to 512 of 46 healthy subjects at rest.
- Patel, A. (2018, June). Generalized Persistence Diagrams. *Journal of Applied and Computational Topology* 1(3-4), 397–419.
- Platt, J. (1998, 07). Sequential minimal optimization: A fast algorithm for training support vector machines. *Advances in Kernel Methods-Support Vector Learning* 208.
- Ramsay, J. O. J. O. (2002). *Applied functional data analysis : methods and case studies*. New York, New York: Springer.
- Ramsay, J. O. J. O. (2005). *Functional data analysis* (2nd ed. ed.). Springer series in statistics. New York: Springer.
- Reininghaus, J., S. Huber, U. Bauer, and R. Kwitt (2015). A stable multi-scale kernel for topological machine learning. In *Proceedings of the IEEE conference on computer vision and pattern recognition*, pp. 4741–4748.
- Robins, V. and K. Turner (2016, November). Principal Component Analysis of Persistent Homology Rank Functions with case studies of Spatial Point Patterns, Sphere Packing and Colloids. *Physica D: Nonlinear Phenomena* 334, 99–117.
- Robinson, A. and K. Turner (2013). Hypothesis testing for topological data analysis.
- Rossi, F., N. Delannay, B. Conan-Guez, and M. Verleysen (2005, mar). Representation of functional data in neural networks. *Neurocomputing* 64, 183–210.
- Saba, T., A. Rehman, M. Shahzad, R. Latif, S. Bahaj, and J. Alyami (2022, 01). Machine learning for post-traumatic stress disorder identification utilizing resting-state functional magnetic resonance imaging. *Microscopy Research and Technique* 85.
- Skraba, P. and K. Turner (2021, March). Wasserstein Stability for Persistence Diagrams. arXiv:2006.16824 [math].
- Szpilrajn, E. (1930). Sur l’extension de l’ordre partiel. *Fundamenta Mathematicae* 16, 386–389. Publisher: Instytut Matematyczny Polskiej Akademii Nauk.
- The RIVET Developers (2020). Rivet.
- Turner, K., Y. Mileyko, S. Mukherjee, and J. Harer (2014, Jul). Fréchet Means for Distributions of Persistence Diagrams. *Discrete & Computational Geometry* 52(1), 44–70.
- Vandaele, R., P. Mukherjee, H. M. Selby, R. P. Shah, and O. Gevaert (2023). Topological data analysis of thoracic radiographic images shows improved radiomics-based lung tumor histology prediction. *Patterns* 4(1), 100657.
- Verri, A., C. Uras, P. Frosini, and M. Ferri (1993). On the use of size functions for shape analysis. *Biological Cybernetics* 70(2), 99–107.
- Vipond, O. (2020). Multiparameter persistence landscapes. *Journal of Machine Learning Research* 21(61), 1–38.
- Xie, S.-Y., P.-W. Wang, H.-J. Zhang, and H.-T. Zhao (2008). Research on the classification of brain function based on svm. In *2008 2nd International Conference on Bioinformatics and Biomedical Engineering*, pp. 1931–1934.

Zomorodian, A. and G. Carlsson (2005, February). Computing Persistent Homology. *Discrete & Computational Geometry* 33(2), 249–274.